

Detection of Epigenomic Network Community Oncomarkers

Thomas E. Bartlett^{1,2,*}, Alexey Zaikin^{1,3,4,5}.

1. Department of Mathematics, University College London, London, United Kingdom.

2. CoMPLEX, University College London, London, United Kingdom.

3. Institute for Women's Health and Department of Mathematics, University College London, London, United Kingdom.

4. Lobachevsky State University of Nizhny Novgorod, Nizhniy Novgorod, Russia.

5. Department of Mathematics, King Abdul Aziz University, Jeddah, Saudi Arabia.

* E-mail: thomas.bartlett.10@ucl.ac.uk

Abstract

In this paper we propose network methodology to infer prognostic cancer biomarkers, based on the epigenetic pattern DNA methylation. Epigenetic processes such as DNA methylation reflect environmental risk factors, and are increasingly recognised for their fundamental role in diseases such as cancer. DNA methylation is a gene-regulatory pattern, and hence provides a means by which to assess genomic regulatory interactions. Network models are a natural way to represent and analyse groups of such interactions. The utility of network models also increases as the quantity of data and number of variables increase, making them increasingly relevant to large-scale genomic studies. We propose methodology to infer prognostic genomic networks from a DNA methylation-based measure of genomic interaction and association. We then show how to identify prognostic biomarkers from such networks, which we term ‘network community oncomarkers’. We illustrate the power of our proposed methodology in the context of a large publicly available breast cancer data-set.

1 Introduction

Complex systems which can be modelled as networks are ubiquitous. Well-known examples include social/communication networks [Beguerisse-Díaz et al., 2014] and economic networks [Saavedra et al., 2014], as well as many others in the biological sciences such as ecological networks [Nandi et al., 2014], gene networks [Wei and Pan, 2010, Li and Wang, 2014], protein networks [Mardia, 2013, Tran and Kwon, 2013], and metabolic networks [Reznik et al., 2013]. Over the past few years in cell biology, much focus has shifted from investigation of individual genes, to pathways of genes, to gene networks. The interest in novel methodology for network analysis in cell biology follows from the recognition that examining the way genes work in groups often yields more accurate inference of biological processes. Further, by considering groups of genes together, a level of statistical significance can be obtained which is not possible when genes are considered individually [Jacob et al., 2012].

Epigenetic patterns are gene-regulatory patterns, meaning that they influence the activity of particular genes, among other phenomena [Jones, 2012]. Epigenetic information can be modulated during the lifetime of an organism by environmental cues [Feinberg et al., 2006, Cooney, 2007, Christensen et al., 2009]. As such, epigenetics can be considered to be an interface between the genome and the environment, and consequently also a conduit for environmental risk factors. Alterations in the epigenetic pattern DNA methylation are among the earliest changes in human carcinogenesis [Feinberg et al., 2006], and hence DNA methylation patterns are expected to yield important prognostic information useful for biomarker development. DNA methylation patterns are thought promising for biomarker development in a wide variety of physiological systems and organs [Verschuur-Maes et al., 2012, Van Hoesel et al., 2013, Fleischer et al., 2014, Kishida et al., 2012, Gao et al., 2013, Kang et al., 2001, 2003, Bhagat et al., 2012, Yamamoto et al., 2012, Luo et al., 2014, Navarro et al., 2012, Maekawa et al., 2013].

It is well established that DNA methylation plays an important role in gene regulation, and hence DNA methylation patterns often reflect gene regulatory behaviour [Jones, 2012]. Changes in DNA methylation are highly stochastic. The time-scale over which these changes take place is much faster than DNA mutations can arise, but much slower than the transient and periodically varying activity of individual genes, and this time-scale is ideal for biomarker development. DNA methylation data are extremely noisy; however, statistics which summarise DNA methylation patterns at the gene level have been shown to have much utility as analytical tools [Bartlett et al., 2013]. It has been shown previously

that DNA methylation can serve as a surrogate measure of genomic-regulatory action [Brocks et al., 2014]. Hence, DNA methylation measurements are a natural basis from which to construct genomic regulatory and related networks. As a cancer progresses, its signalling and control networks are re-arranged (‘re-wired’), leading to genomic changes which are advantageous for the cancer [Barabási and Oltvai, 2004]. Previous research has found that patient survival outcome in breast cancer can be predicted well by network models of this re-wiring, based on gene expression data [Taylor et al., 2009]. Hence, network models based on DNA methylation measurements are a very promising basis for the development of prognostic biomarkers.

Statistical network models are a parsimonious way to represent and analyse large numbers of variables and samples. They are efficient analytical tools appropriate for the very large data-sets which are produced by the latest technologies in cell biology. When carrying out modelling of this type, it is important to balance statistical fidelity with computational efficiency. The ‘stochastic blockmodel’ (SBM) [Holland et al., 1983, Bickel and Chen, 2009] is an efficient network model which has been widely studied and is well understood, and hence it is a good basis for our proposed methodology. Under the SBM, there is a greater probability of observing an edge (or interaction) between a pair of nodes if they are in the same block, or community. The Newman-Girvan modularity [Newman and Girvan, 2004] quantifies the extent to which network edges are observed between community members, for a particular assignment of nodes to communities, compared to the expected number of edges between community members if there were no community structure present. It can be shown that, under certain conditions, fitting the stochastic blockmodel is equivalent to maximising the Newman-Girvan modularity over a network, and that these are both equivalent to spectral clustering [Riolo and Newman, 2012, Bickel and Chen, 2009]. We use spectral clustering as an efficient computational algorithm for fitting the SBM.

The problem of finding communities in biological networks has been studied for many years [Girvan and Newman, 2002]. Genomic networks can be decomposed into subnetwork modules, which are functional units with specific biological roles [Shen-Orr et al., 2002]. Hence, the communities detected by the SBM in a genomic network can be thought of as subnetwork modules with specific physiological functions. It has been shown recently that, under reasonable assumptions, the SBM can be used to represent any network as a ‘network histogram’, whatever the generating mechanism of that network. Further, the network histogram provides a heuristic method to estimate the optimum number of blocks, or clusters, which a valid blockmodel representation of the network may contain. This is important and useful, because it means that the blockmodel can be used to identify an unknown number of communities, or functional subnetwork modules, in a biological network. Genomic networks are typically scale-free, which means that they exhibit a power-law degree distribution [Wagner, 2002]. Further, they are thought to be hierarchical [Barabási and Oltvai, 2004, Palla et al., 2010], displaying multi-scale properties. This means that different functional organisation is visible at different granularities, or scales. We use the network histogram method [Olhede and Wolfe, 2014] to estimate the optimal granularity at which to identify communities, or functional subnetwork modules, in our prognostic networks by fitting the SBM.

This paper is organised as follows. In section 2, we describe our DNA methylation based measure of interaction or association between pairs of genes, called the ‘DNA methylation network interaction measure’, and we show how to use this measure to infer prognostic genomic networks. An edge between a pair of genes/nodes in these networks indicates that the strength of interaction or association between those genes is associated with disease progression. Also in section 2, we show how to identify prognostic biomarkers from such networks, using community detection to identify subnetwork modules within the network. These communities are groups of nodes/genes among which there is a high density of prognostic interactive or associative behaviour, and we term them ‘network community oncomarkers’. In section 3, we demonstrate the utility of our proposed methodology in the context of a large, publicly available breast cancer data-set. To do so, we use each network community oncomarker to calculate a one-number prognostic score for each patient, and we use these scores to classify patients one by one into prognostic groups. Also in section 3, we show that among the genes of the network community oncomarkers, the DNA methylation network interaction measure is associated with co-regulatory behaviour as measured by gene expression, justifying these findings in terms of biological function.

2 Proposed methodology

An overview of our proposed methodology appears in figure 1, following which the component parts of this methodology are described in detail.

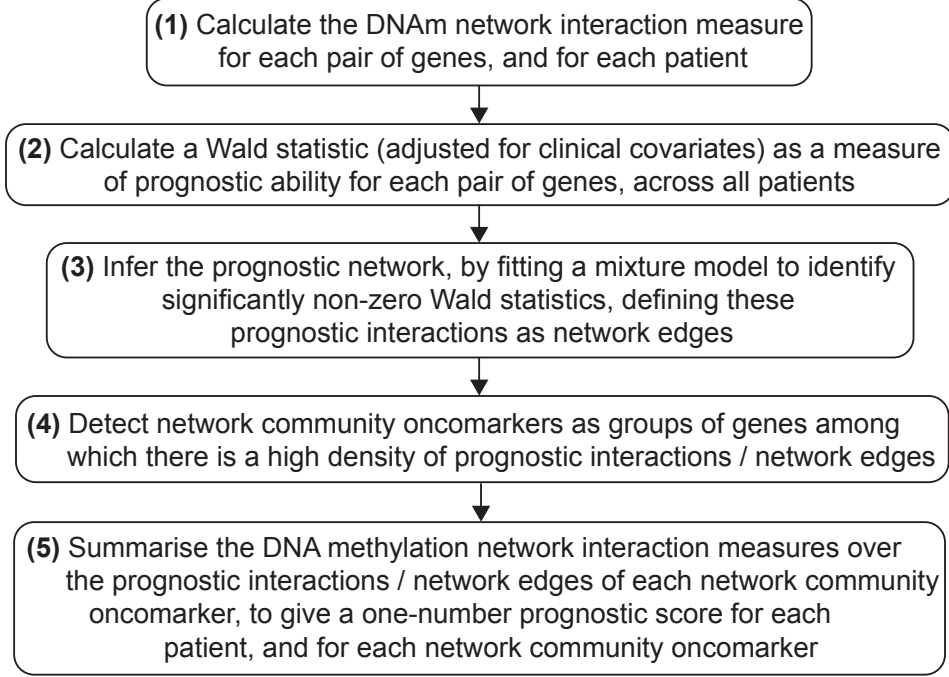


Figure 1: Overview of methods.

2.1 DNA Methylation Network Interaction Measure

DNA methylation is a chemical modification to DNA which may occur at numerous locations within a gene: the pattern of these modifications within a gene forms a ‘DNA methylation profile’. Using canonical correlation analysis (CCA) [Hotelling, 1936] we previously proposed a statistic [Bartlett et al., 2014] which measures the strength of interaction or association between a pair of genes (network nodes) in a single sample/patient, based on DNA methylation profiles (figure 2). This statistic quantifies the extent to which the DNA methylation profiles of a pair of genes explain each other. It is based only on measurements of the DNA methylation profiles of that pair of genes, and it acts as a surrogate for a measure of the extent to which this pair of genes behave interactively or associatively. Such behaviour may include transcriptional regulation or co-regulation, or other types of biochemical interaction, influencing gene expression levels, isoforms and the presence of alternatively spliced gene products, among other phenomena [Jones, 2012]. The details of this DNA methylation network interaction measure are as follows.

The DNA methylation network interaction measure is defined by analogy to CCA. CCA aims to discover linear combinations of variables of one type, and linear combinations of variables of another type, so that these combinations best explain each other. In this context, a particular way of combining (by scaling and adding) the deviations from the mean methylation profile at a number of locations within one gene might be particularly effective at explaining a particular combination of (again, by scaling and adding) the deviations from the mean methylation profile at a number of locations in another gene, and *vice-versa*. There will probably be fewer ways in which the methylation levels of these genes covary across the samples than there are locations at which methylation is measured along the genes; this is because the methylation level is highly correlated at many locations along a particular gene. CCA finds the most important components of this covariation across samples.

CCA seeks to find the vectors a and b , in the p and q dimensional spaces of variables $\mathbf{X} = (x_1, x_2, \dots, x_p)'$ and $\mathbf{Y} = (y_1, y_2, \dots, y_q)'$ respectively, which maximise the correlation $\rho = \text{cor}(\mathbf{a}'\mathbf{X}, \mathbf{b}'\mathbf{Y})$ defined accord-

ing to equation 1:

$$\rho = \frac{\mathbf{a}'\Sigma_{XY}\mathbf{b}}{\sqrt{\mathbf{a}'\Sigma_{XX}\mathbf{a}}\sqrt{\mathbf{b}'\Sigma_{YY}\mathbf{b}}}, \quad (1)$$

where $\Sigma_{XX} = \mathbb{E}[(\mathbf{X} - \boldsymbol{\mu}_X)(\mathbf{X} - \boldsymbol{\mu}_X)']$ and $\Sigma_{YY} = \mathbb{E}[(\mathbf{Y} - \boldsymbol{\mu}_Y)(\mathbf{Y} - \boldsymbol{\mu}_Y)']$ are the covariance matrices of \mathbf{X} and \mathbf{Y} respectively, $\Sigma_{XY} = \mathbb{E}[(\mathbf{X} - \boldsymbol{\mu}_X)(\mathbf{Y} - \boldsymbol{\mu}_Y)']$ is the cross-covariance matrix of \mathbf{X} and \mathbf{Y} , and $\boldsymbol{\mu}_X$ and $\boldsymbol{\mu}_Y$ are the mean vectors of \mathbf{X} and \mathbf{Y} .

Two genes X and Y have corresponding methylation profiles which are measured for sample / patient k at p and q CpGs (loci) respectively along these genes. Denoting these measurements by the variables x_1, \dots, x_p and y_1, \dots, y_q for genes X and Y respectively, the DNA methylation profiles for these genes, for patient k , can be represented by the vectors $\mathbf{x}(k)$ and $\mathbf{y}(k)$, which have p and q entries respectively. A measure of DNA methylation network interaction $\rho_{XY}(k)$, of the methylation profiles of genes X and Y for sample k , can then be defined by analogy with equation 1, according to equation 2:

$$\rho_{XY}(k) = \frac{\mathbf{x}(k)^T \hat{\Sigma}_{XY}^{(h)} \mathbf{y}(k)}{\sqrt{\mathbf{x}(k)^T \hat{\Sigma}_{XX}^{(h)} \mathbf{x}(k)} \sqrt{\mathbf{y}(k)^T \hat{\Sigma}_{YY}^{(h)} \mathbf{y}(k)}}, \quad (2)$$

where $\hat{\Sigma}_{XX}^{(h)}$, $\hat{\Sigma}_{YY}^{(h)}$ and $\hat{\Sigma}_{XY}^{(h)}$ are estimated from healthy rather than cancer samples in the methylation data set, according to equations 3 - 5,

$$\hat{\Sigma}_{XX}^{(h)} = \frac{1}{n_h} \sum_{k \in \text{healthy}} \left(\mathbf{x}(k) - \hat{\boldsymbol{\mu}}_X^{(h)} \right) \left(\mathbf{x}(k) - \hat{\boldsymbol{\mu}}_X^{(h)} \right)^T \quad (3)$$

$$\hat{\Sigma}_{YY}^{(h)} = \frac{1}{n_h} \sum_{k \in \text{healthy}} \left(\mathbf{y}(k) - \hat{\boldsymbol{\mu}}_Y^{(h)} \right) \left(\mathbf{y}(k) - \hat{\boldsymbol{\mu}}_Y^{(h)} \right)^T \quad (4)$$

$$\hat{\Sigma}_{XY}^{(h)} = \frac{1}{n_h} \sum_{k \in \text{healthy}} \left(\mathbf{x}(k) - \hat{\boldsymbol{\mu}}_X^{(h)} \right) \left(\mathbf{y}(k) - \hat{\boldsymbol{\mu}}_Y^{(h)} \right)^T, \quad (5)$$

where

$$\hat{\boldsymbol{\mu}}_X^{(h)} = \frac{1}{n_h} \sum_{k \in \text{healthy}} \mathbf{x}(k),$$

and

$$\hat{\boldsymbol{\mu}}_Y^{(h)} = \frac{1}{n_h} \sum_{k \in \text{healthy}} \mathbf{y}(k),$$

and n_h is the number of healthy samples in the data set. When the DNA methylation network interaction measure $\rho_{XY}(k)$ is large (i.e., close to 1), the corresponding pair of genes explain each others' gene-regulatory behaviour (as reflected in their methylation profiles) well, or have otherwise well-correlated interactive or associative behaviour, for sample/patient k . Hence, $\rho_{XY}(k)$ measures (according to their DNA methylation profiles) the level of interaction or association between genes X and Y in tumour sample k , compared to typical interactions between these genes in healthy tissue.

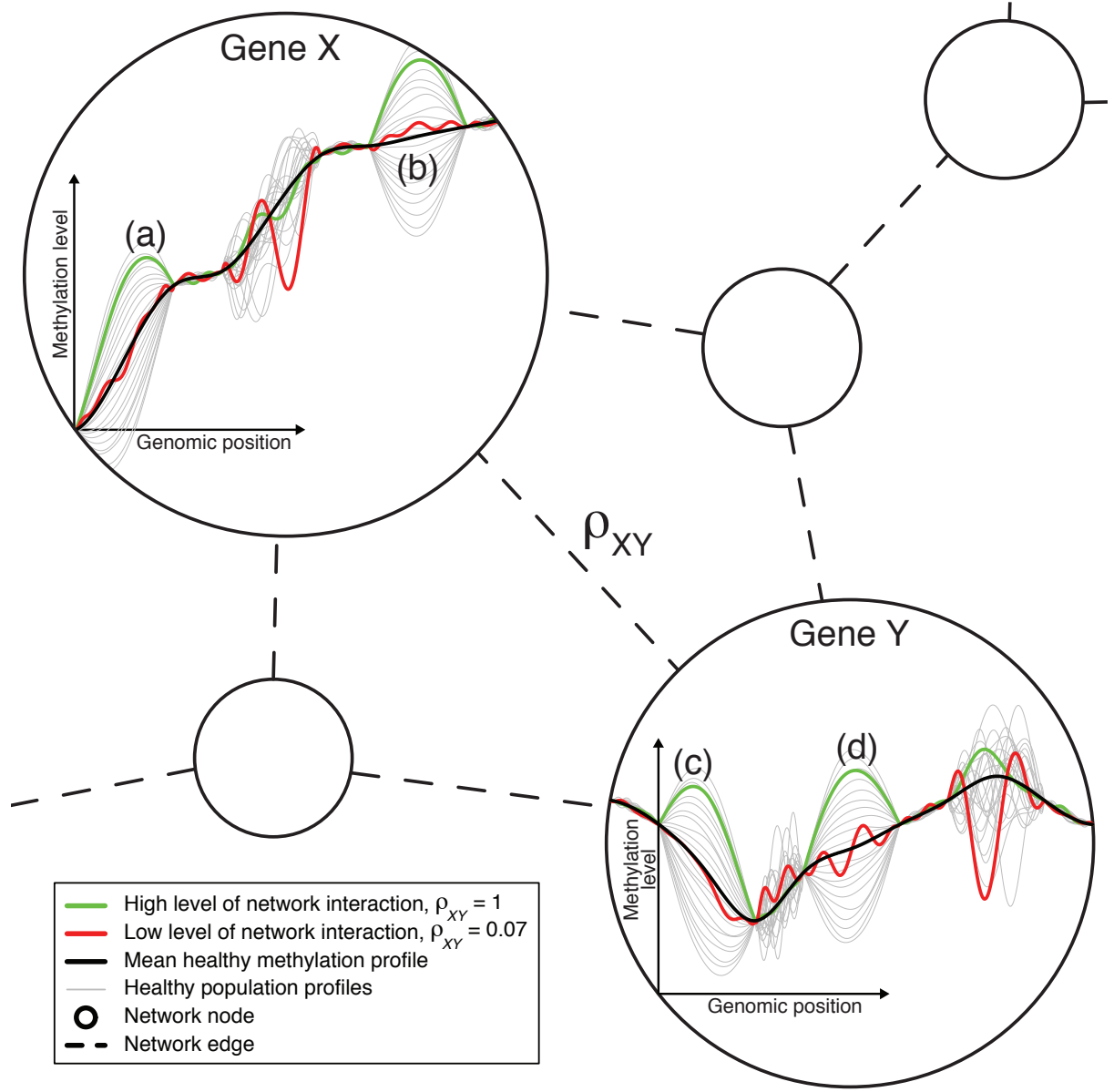


Figure 2: The DNA methylation network interaction measure.

A combination of the variation of the healthy methylation profiles in regions (a) and (b) of gene X explains well / is well-explained by a combination of the variation of the healthy methylation profiles in regions (c) and (d) of gene Y. The green cancer sample varies by a large amount about the mean methylation profile and in a typical way in these regions in both genes. Hence, the green sample corresponds to a high level of network interaction for this sample, $\rho_{XY} = 1$. The equivalent variations in the other regions of these genes do not explain each other well, and so the red sample, which varies by a large amount in these other regions and varies less and in an atypical way in regions (a) - (d), corresponds to a low level of network interaction, $\rho_{XY} = 0.07$. Genes X and Y are likely to have different numbers of methylation measurement locations (i.e., variables X and Y are of different dimension). The ordering of the measurement locations has no influence on the calculation of ρ , as long as the ordering is consistent across samples.

2.2 Prognostic Network Construction

Our proposed methodology for inference of network oncomarkers is based on a prognostic interaction network over m genes. This network is represented by the $m \times m$ adjacency matrix \mathbf{A} , in which an edge is defined to be present (i.e., $A_{ij} = 1$) if and only if the corresponding pair of genes (nodes) are prognostic according to the DNA methylation network interaction measure of section 2.1. Otherwise, we set $A_{ij} = 0$. N.B., i and j are now redefined compared to the last section, so that they index genes rather than DNA methylation locations. This formulation will not be problematic, because all subsequent analysis is carried out at the level of genes rather than DNA methylation locations. To identify prognostic edges, we use the Cox proportional hazards model [Cox, 1972] to calculate a Wald-statistic z_{ij} for each of the $\binom{m}{2}$ pairs of genes in the network. The Wald statistic quantifies the strength of association of the DNA methylation network interaction measure ρ_{ij} for the pair of genes i and j ($i = 1, \dots, m$ and $j = 1, \dots, m$) with patient survival outcome across patients k ($k = 1, \dots, n$). We use a multivariate Cox model, adjusting these Wald statistics for clinical covariates. We adjust in this way in order to detect novel DNA methylation biomarkers which are independent of known prognostic clinical features.

The Wald statistic is asymptotically normally distributed with unit variance [Harrell, 2001], and we can therefore model the distribution of our observed Wald statistics, z_{ij} , as a mixture of Gaussians. We have previously demonstrated the utility of mixture modelling to a related network inference problem [Bartlett, 2015], and a similar approach can be applied in this context. We model the z_{ij} as a Gaussian mixture as follows:

$$z_{ij} \sim \begin{cases} \mathcal{N}(\mu_{ij}, \sigma^2), & \text{if } A_{ij} = 1, \\ \mathcal{N}(0, \sigma^2), & \text{if } A_{ij} = 0, \end{cases} \quad (6)$$

where $\mathcal{N}(\mu_{ij}, \sigma^2)$ is the normal distribution. We fit this mixture model to each observed statistic z_{ij} , and then infer whether, given z_{ij} , it is more likely that $\mu_{ij} = 0$, or $\mu_{ij} \neq 0$, leading to the estimates $\hat{A}_{ij} = 0$ or $\hat{A}_{ij} = 1$ respectively. We fit this model using the empirical Bayes procedure [Johnstone and Silverman, 2004], defining a mixture prior distribution $f_{\text{prior}}(\mu_{ij})$ over the μ_{ij} of equation 6:

$$f_{\text{prior}}(\mu_{ij}) = (1 - w) \delta(\mu_{ij}) + w \gamma(\mu_{ij}), \quad (7)$$

where w is the mixing parameter between the two components, which can also be interpreted as $w = \mathbb{E}[p(A_{ij} = 1)]$, and $\gamma(\cdot|a)$ is the Laplace probability density function,

$$\gamma(\mu_{ij}|a) = \frac{a}{2} \exp(-a |\mu_{ij}|),$$

where we use the standard value of $a = 0.5$ [Johnstone and Silverman, 2004]. Taking the mixture components to have Gaussian likelihoods, $f_{\mathcal{N}}(\cdot|\mu_{ij}, \sigma^2)$, as in equation 6, it follows from equation 7 that the posterior density over the observed prognostic Wald statistic z_{ij} is:

$$f_{\text{posterior}}(\mu_{ij}|z_{ij}) = \frac{(1 - w) \delta(\mu_{ij}) f_{\mathcal{N}}(z_{ij}|0, \sigma^2) + w \gamma(\mu_{ij}) f_{\mathcal{N}}(z_{ij}|\mu_{ij}, \sigma^2)}{f_{\text{marginal}}(z_{ij})}, \quad (8)$$

where the marginal density is:

$$f_{\text{marginal}}(z_{ij}) = (1 - w) f_{\mathcal{N}}(z_{ij}|0, \sigma^2) + w g(z_{ij}), \quad (9)$$

where $g(\mu_{ij})$ is the convolution of the Laplace density with the standard normal density. If the Laplace distribution in the prior (equation 7) were replaced with a Gaussian, then the marginal distribution (equation 9) would be a mixture of Gaussians. However, as noted previously [Johnstone and Silverman, 2004], this empirical Bayes procedure requires a prior with tails that are exponential or heavier. Hence, we similarly use the Laplace rather than Gaussian prior which is a slight model mis-specification.

Although a separate model is fitted to each observed Wald statistic z_{ij} , a common weight w_i is used for each gene/node i . This estimate of w_i is found as the value which maximises the marginal likelihood (equation 10) of the observed statistics z_{ij} over all the pairwise comparisons of i with j , $j \neq i$. This allows the model for each such pairwise comparison (i, j) to ‘borrow strength’ from all the other comparisons (i, j') , $j' \neq i$, $j' \neq j$:

$$\hat{w}_i = \arg \max_w \sum_{j \neq i} \log \{ (1 - w) \phi(z_{ij}) + w g(z_{ij}) \}. \quad (10)$$

For a particular gene i , if the z_{ij} are mostly close to zero, then w_i will be set low, which means that fewer edges ($A_{ij} = 1$) will be detected; this hence corresponds to i being a low-degree node. If for a different gene i the z_{ij} are generally further from zero, then \hat{w}_i will be set high, which corresponds more edges being detected; this hence corresponds to i being a high-degree node. Therefore, setting \hat{w}_i separately for each gene i allows adaptation to a heterogenous degree distribution in \mathbf{A} . As previously [Johnstone and Silverman, 2004], we use the posterior median to obtain the estimate $\hat{\mu}_{ij}$. Then we make a conservative estimate of \mathbf{A} as follows:

$$\begin{aligned}\hat{A}_{ij} &= 1 && \text{if } \hat{\mu}_{ij} > 0 \text{ and } \hat{\mu}_{ji} > 0 \quad \text{or} \quad \hat{\mu}_{ij} < 0 \text{ and } \hat{\mu}_{ji} < 0, \\ \hat{A}_{ij} &= 0 && \text{otherwise.}\end{aligned}\tag{11}$$

2.3 Community and Oncomarker Detection

Network nodes can be grouped together according to their propensity to interact with each other, for example groups of friends in a social network, or functional subnetwork modules in a biological network; this method is referred to as community detection [Girvan and Newman, 2002, Newman, 2004]. We use community detection to naturally infer groups of genes in our constructed prognostic network. These groups of genes interact differently in cancer than in healthy tissue, in a way which is predictive of how advanced the disease is. We term these groups ‘network community oncomarkers’. Within a network community oncomarker the genes may interact with each other more (relative to healthy tissue) the more serious the disease is (as in figure 6c), or they may interact with each other less the more serious the disease is, (as in figure 6a). We carry out the task of community detection by fitting the degree-corrected stochastic blockmodel [Holland et al., 1983, Bickel and Chen, 2009]. We fit this model in an efficient way by regularised spectral clustering [Qin and Rohe, 2013], calculating the optimum number of communities to divide the network into by the network histogram method [Olhede and Wolfe, 2014]. Each community identified in this way represents a potential network community oncomarker.

For each network community oncomarker, we then calculate a prognostic score for each patient, by summarising the DNA methylation network interaction measure over this group of genes. This prognostic score can be used as a one-number summary of disease prognosis for that patient according to that network community oncomarker. The following points are important when calculating these summaries. Some gene-gene interactions will correspond to an increasingly negative DNA methylation network interaction measure ρ_{ij} for worse patient prognosis. On the other hand, some gene-gene interactions will correspond to an increasingly positive ρ_{ij} for worse prognosis. This means that care must be taken when summarising the network interaction measure across the network community oncomarker. Also, for the same amount of prognostic information conveyed, the magnitude of the changes in the network interaction measure may not be the same for each prognostic pairs of genes. To address these points, we combine the ρ_{ij} across the prognostic pairs of genes of the network community after first multiplying them by the corresponding fitted Cox proportional hazards model coefficients $\hat{\theta}_{ij}$, obtained as described at the start of section 2.2. Under the Cox proportional hazards model, the fitted model coefficient $\hat{\theta}_{ij}$ for a predictor ij gives the log of the hazard-ratio (HR) for that predictor in the model, i.e., $\log(\text{HR}_{ij}) = \hat{\theta}_{ij}$. The hazard ratio is the scale-factor increase in probability of an event (e.g., death) occurring per unit time, relative to the baseline hazard (e.g., compared to a control group). Hence, these coefficients are interpretable in the same way, without scaling issues, across fitted models. This means that, for patient k , we can combine the DNA methylation network interaction measures over a network community oncomarker to generate a one-number prognostic score, as follows:

$$\text{Score}_k = \sum_{i \in C, j \in C, i < j} \hat{A}_{ij} \hat{\theta}_{ij} \rho_{ij}(k),$$

where C is the set of nodes in the network community oncomarker, $\hat{\mathbf{A}}$ is the inferred adjacency matrix, $\rho_{ij}(k)$ is the DNA methylation network interaction measure for genes/nodes i and j and patient k , and $\hat{\theta}_{ij}$ is the corresponding fitted Cox multivariate proportional-hazards model coefficient. Network edges/DNA methylation network interaction measures ρ_{ij} which increase with poor prognosis (i.e., pairs of genes which interact more as the disease progresses, coloured green in figure 6), will correspond to $\hat{\theta}_{ij} > 0$. Hence, an increase in such a ρ_{ij} will increase the prognostic score. Equivalently, network edges/DNA methylation network interaction measures ρ_{ij} which decrease with poor prognosis (i.e., pairs

of genes which interact less as the disease progresses, coloured red in figure 6), will correspond to $\hat{\theta}_{ij} < 0$. Hence, a decrease in such a ρ_{ij} will also increase the prognostic score.

2.4 An equivalent gene-expression interaction measure

To examine further the hypothesis that the DNA methylation network interaction measure is a reflection of co-regulatory or co-regulated gene-expression patterns (among other genomic effects), we need an equivalent measure of gene-gene interaction or association in terms of gene expression. We can calculate such a measure, $\rho_{XY}^{\text{expr}}(k)$, for gene expression measurements $x^{\text{expr}}(k)$ and $y^{\text{expr}}(k)$ for the genes X and Y and patient k , as follows (equation 12):

$$\rho_{XY}^{\text{expr}}(k) = \frac{\left(x^{\text{expr}}(k) - \hat{\mu}_{x^{\text{expr}}}^{(h)}\right)}{\hat{\sigma}_{x^{\text{expr}}}^{(h)}} \cdot \frac{\left(y^{\text{expr}}(k) - \hat{\mu}_{y^{\text{expr}}}^{(h)}\right)}{\hat{\sigma}_{y^{\text{expr}}}^{(h)}} \quad (12)$$

where

$$\begin{aligned} \hat{\mu}_{x^{\text{expr}}}^{(h)} &= \frac{1}{n_h} \sum_{k \in \text{healthy}} x^{\text{expr}}(k) \quad \text{and} \quad \hat{\mu}_{y^{\text{expr}}}^{(h)} = \frac{1}{n_h} \sum_{k \in \text{healthy}} y^{\text{expr}}(k), \\ \left(\hat{\sigma}_{x^{\text{expr}}}^{(h)}\right)^2 &= \frac{1}{n_h} \sum_{k \in \text{healthy}} \left(x^{\text{expr}}(k) - \hat{\mu}_{x^{\text{expr}}}^{(h)}\right)^2 \quad \text{and} \quad \left(\hat{\sigma}_{y^{\text{expr}}}^{(h)}\right)^2 = \frac{1}{n_h} \sum_{k \in \text{healthy}} \left(y^{\text{expr}}(k) - \hat{\mu}_{y^{\text{expr}}}^{(h)}\right)^2. \end{aligned}$$

The intuition of equation 12 is that when the gene expression measurements $x^{\text{expr}}(k)$ and $y^{\text{expr}}(k)$ deviate *in the same sample* from the corresponding healthy mean expression levels, this measure will be non-zero. When this occurs in the same samples as the DNA methylation network interaction measure $\rho_{XY}(k)$ is also non-zero, we will see a correlation between $\rho_{XY}(k)$ and ρ_{XY}^{expr} . These interaction measures for methylation and expression, $\rho_{XY}(k)$ and ρ_{XY}^{expr} , are equivalent because they both measure deviation from typical interactive behaviour in healthy/control samples. We note that, that while ρ_{XY}^{expr} works satisfactorily for this comparison, it would not be expected to be a sensitive statistic to use as a prognostic tool.

3 Examples

We present an example application of the methodology proposed in section 2 to a large publicly available breast cancer invasive carcinoma (BRCA) data-set downloaded from the Cancer Genome Atlas (TCGA). We downloaded an initial batch of DNA methylation data for tumour samples taken from 175 individuals (the training set), together with clinical data for these samples relating to patient survival outcome, and the covariates age, disease stage, and residual disease. These training data were used to detect potential network community oncomarkers. We then downloaded DNA methylation data for a further 528 tumour samples (the test set), together with data for the same clinical features: these independent samples were used to validate the potential network community oncomarkers. We also downloaded corresponding DNA methylation data for healthy breast tissue samples from 98 individuals to form a reference population of DNA methylation profiles for this analysis, and we downloaded gene expression data for 216 of the tumours for which DNA methylation data were also available.

We inferred the binary prognostic adjacency matrix \mathbf{A} for the 175 samples of the BRCA training data set according to the methods set out in sections 2.1 - 2.2. DNA methylation data were available for 14829 genes, and hence the number of nodes/genes m in the inferred adjacency matrix $\hat{\mathbf{A}}$ is $m = 14829$. The presence of an edge in $\hat{\mathbf{A}}$, i.e. $\hat{A}_{ij} = 1$, indicates that the interaction between genes i and j is associated with disease progression. The edge density of $\hat{\mathbf{A}}$ is 0.0035, i.e. $p(\hat{A}_{ij} = 1) = 0.0035$. We then extracted the connected component from this inferred network and carried out community detection on this connected component as described in section 2.3. This resulted in 33 communities ranging from 116 to 285 nodes in size. The reduced adjacency matrix relating to these communities (with $m = 5668$ and $p(\hat{A}_{ij} = 1) = 0.023$) is shown in figure 3.

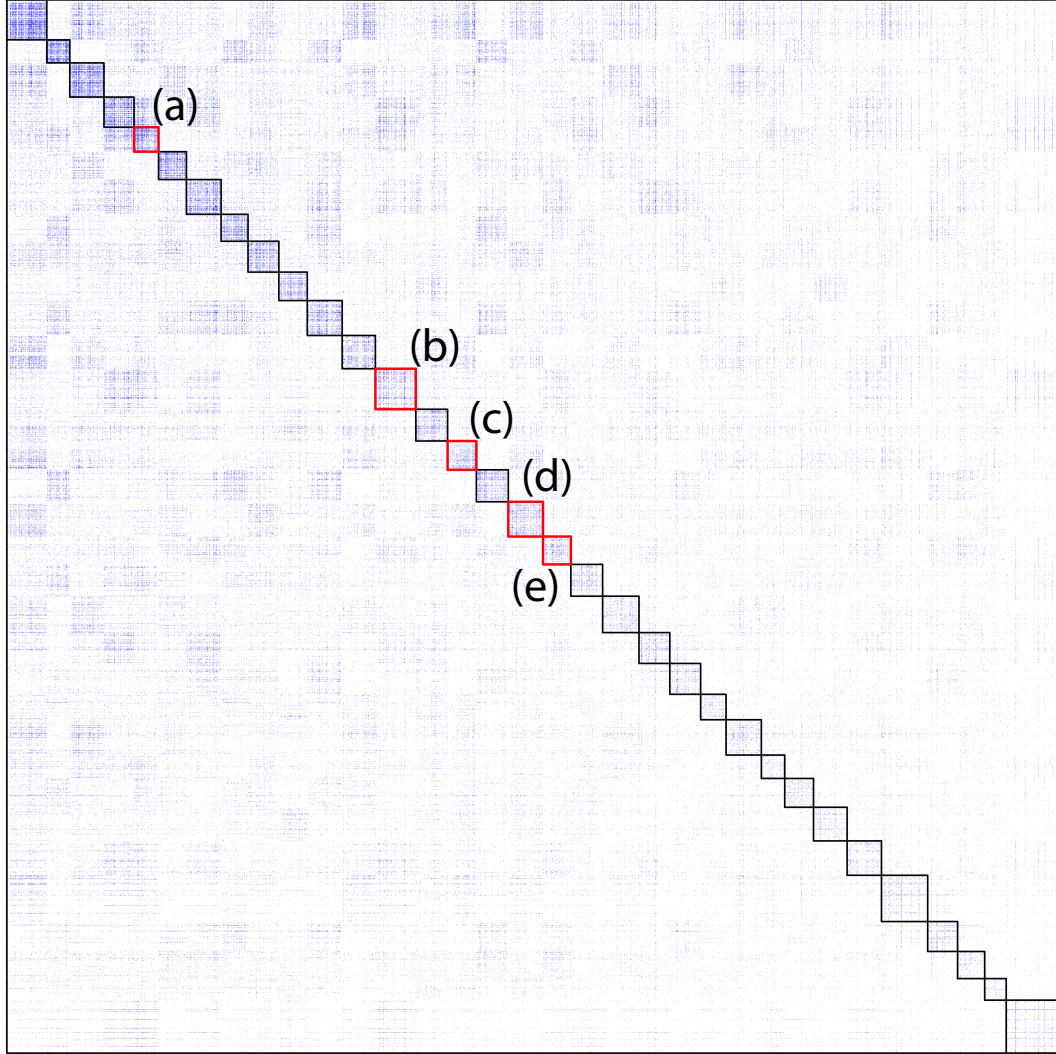


Figure 3: The inferred prognostic adjacency matrix after community detection. Entries in the adjacency matrix equal to 1 (representing a network edge) are coloured blue. Detected communities are outlined in black. The potential network community oncomarkers which are analysed further in figures 4 - 7 and tables 1 - 2 and S1 - S5 are outlined in red, and labelled (a) - (e).

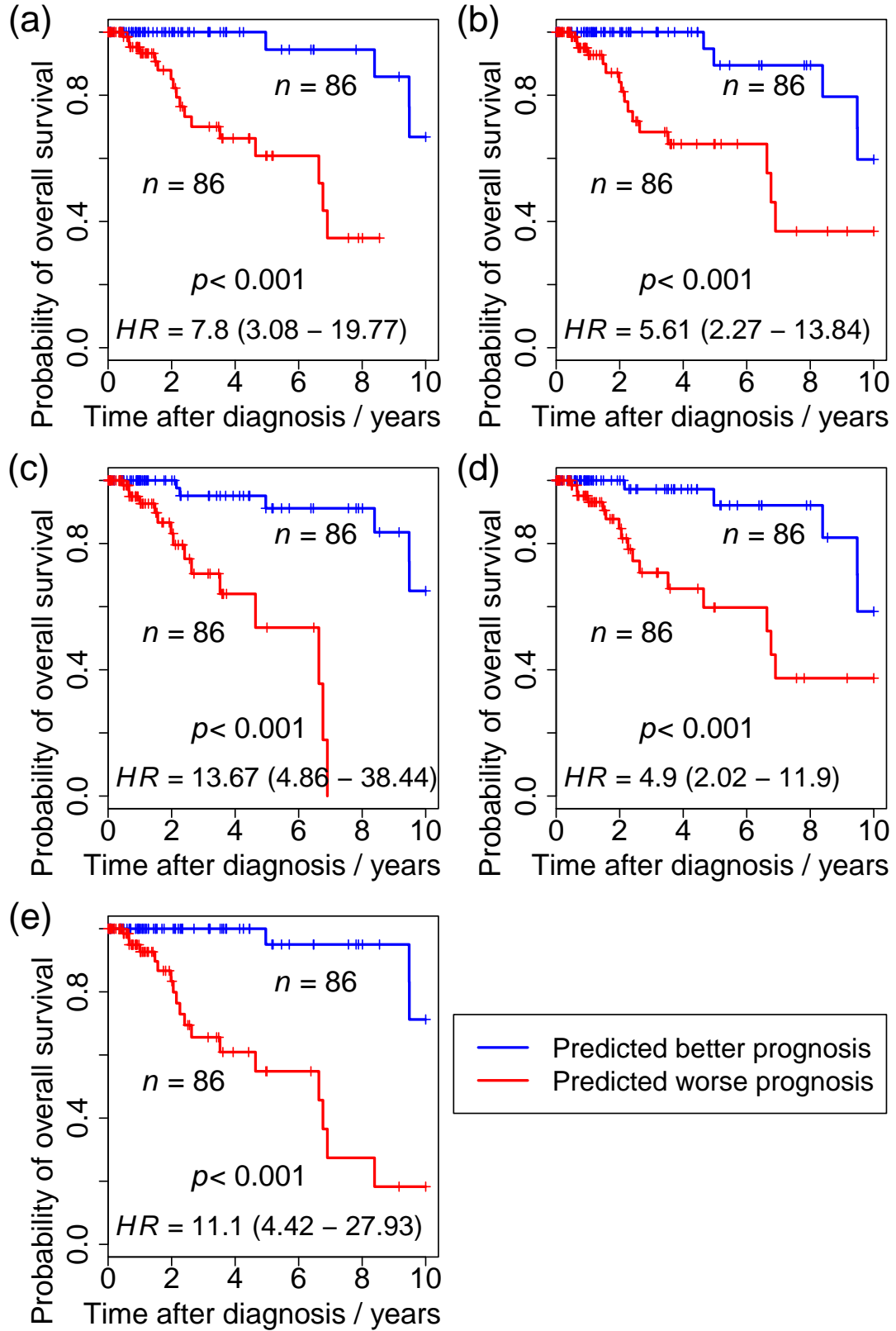


Figure 4: Network community oncomarkers: Kaplan-Meier plots for the training set. Comparison of survival curves for the patient groups defined by the prognostic score for each network community oncomarker. The groups are divided by the median prognostic score in the 175 samples of the training data set. The hazard ratio (HR) is displayed with 95% C.I. in brackets, with the corresponding p-value calculated by univariate Cox regression. (a) - (e) indicate network community oncomarkers 1 - 5, as shown in figure 3.

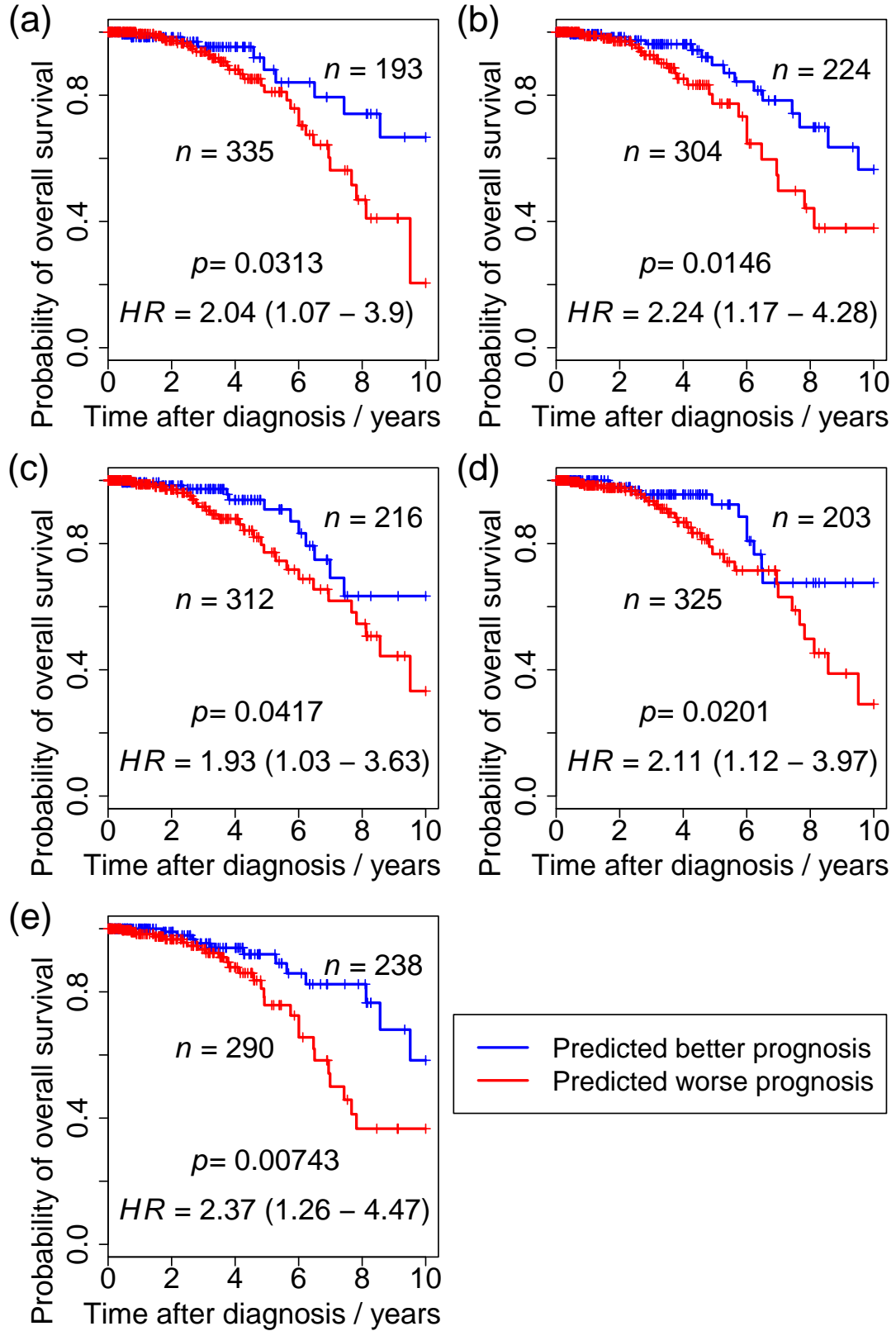


Figure 5: Network community oncomarkers: Kaplan-Meier plots for the test / validation set. Comparison of survival curves for the patient groups defined by the prognostic score for each network community oncomarker. The groups are divided by the median prognostic score in the 175 samples of the training data set. The hazard ratio (HR) is displayed with 95% C.I. in brackets, with the corresponding p-value calculated by univariate Cox regression. (a) - (e) indicate network community oncomarkers 1 - 4, as shown in figure 3.

We validated each of the 33 potential network community oncomarkers in the 528 independent tumour samples of the test/validation set. We note that these 528 samples were not used in any way to identify the 33 potential network community oncomarkers shown in figure 3. Hence in this validation each of these 528 patients were classified individually according to prognosis without reference to the other validation samples. This means that comparing these prognostic classifications assigned to the validation samples is a true test of prognostic ability of the network community oncomarkers. To carry out the validation, we calculated the prognostic score for the 528 independent/unseen samples of the test set, based on the inferred prognostic adjacency matrix $\hat{\mathbf{A}}$ and the fitted Cox multivariate proportional hazards model coefficients $\hat{\boldsymbol{\theta}}$ obtained from the initial 175 samples of the training set. Using this trained model, we calculated one prognostic score for each potential network community oncomarker for each of the 528 unseen test-set samples. We then tested the prognostic score, for each potential network community oncomarker, for significant prediction of patient survival outcome in these 528 unseen test-set samples. The five potential network community oncomarkers which validated in this way with the highest level of significance are outlined in red in figure 3. The results of univariate and multivariate Cox regression for these five best network community oncomarkers are shown in figures 4 and 5, and in tables 1 and 2, for the training and test sets respectively. For the multivariate analysis, samples with missing data for any of the clinical covariates were removed, leaving 172 and 396 samples for the training and test sets respectively.

	HR (95%CI)	p	n
Prognostic Score	77.1 (10.5-567)	<0.001	172
Age	1.79 (0.66-4.84)	0.249	172
Residual Disease	15.4 (4.68-50.9)	<0.001	172
Stage	2.85 (0.96-8.46)	0.060	172

(a) Network community oncomarker 1.

	HR (95%CI)	p	n
Prognostic Score	51.3 (8.35-315)	<0.001	172
Age	1.42 (0.48-4.23)	0.53	172
Residual Disease	30.4 (5.82-158)	<0.001	172
Stage	1.95 (0.68-5.54)	0.212	172

(b) Network community oncomarker 2.

	HR (95%CI)	p	n
Prognostic Score	50.1 (9.77-256)	<0.001	172
Age	2.16 (0.81-5.8)	0.125	172
Residual Disease	13.3 (4.54-39.1)	<0.001	172
Stage	2.41 (0.81-7.18)	0.114	172

(c) Network community oncomarker 3.

	HR (95%CI)	p	n
Prognostic Score	22.7 (5.52-93.1)	<0.001	172
Age	3.49 (1.3-9.42)	0.0135	172
Residual Disease	16.3 (5.24-50.7)	<0.001	172
Stage	1.05 (0.38-2.91)	0.928	172

(d) Network community oncomarker 4.

	HR (95%CI)	p	n
Prognostic Score	46.0 (8.17-259)	<0.001	172
Age	2.91 (1-8.44)	0.0493	172
Residual Disease	7.04 (2.68-18.5)	<0.001	172
Stage	3.74 (1.23-11.4)	0.02	172

(e) Network community oncomarker 5.

Table 1: Network community oncomarkers - training set prognosis.

Multivariate Cox regression was used to test significance of the prognostic scores obtained from the network community oncomarkers. (a) - (e) indicate network community oncomarkers 1 - 5, as shown in figure 3.

	HR (95%CI)	<i>p</i>	<i>n</i>
Prognostic Score	4.89 (1.65-14.5)	0.00429	396
Age	3.52 (1.46-8.49)	0.00513	396
Residual Disease	12.5 (5.32-29.3)	<0.001	396
Stage	1.62 (0.66-4)	0.294	396

(a) Network community oncomarker 1.

	HR (95%CI)	<i>p</i>	<i>n</i>
Prognostic Score	5.07 (1.81-14.1)	0.00195	396
Age	3.67 (1.49-9.03)	0.00458	396
Residual Disease	8.72 (3.78-20.1)	<0.001	396
Stage	1.47 (0.6-3.61)	0.406	396

(b) Network community oncomarker 2.

	HR (95%CI)	<i>p</i>	<i>n</i>
Prognostic Score	2.63 (1.01-6.89)	0.0484	396
Age	2.07 (0.86-5)	0.106	396
Residual Disease	11.3 (4.97-25.5)	<0.001	396
Stage	2.04 (0.76-5.45)	0.157	396

(c) Network community oncomarker 3.

	HR (95%CI)	<i>p</i>	<i>n</i>
Prognostic Score	4.92 (1.8-13.5)	0.00189	396
Age	1.91 (0.78-4.69)	0.159	396
Residual Disease	17.2 (6.76-43.9)	<0.001	396
Stage	0.92 (0.34-2.48)	0.871	396

(d) Network community oncomarker 4.

	HR (95%CI)	<i>p</i>	<i>n</i>
Prognostic Score	2.5 (0.94-6.65)	0.0668	396
Age	2.23 (0.94-5.27)	0.0677	396
Residual Disease	8.17 (3.47-19.3)	<0.001	396
Stage	1.59 (0.64-3.95)	0.321	396

(e) Network community oncomarker 5.

Table 2: Network community oncomarkers - test/validation set prognosis.

Multivariate Cox regression was used to test significance of the prognostic scores obtained from the network community oncomarkers. (a) - (e) indicate network community oncomarkers 1 - 5, as shown in figure 3.

Figure 6 shows the five network community oncomarkers which validated most significantly. Green edges indicate gene-gene interactions which become stronger with disease progression. Red edges indicate interactions which become weaker with disease progression. Hence, the network community oncomarkers of figures 6a and figure 6b can be considered to be functional subnetwork modules which becomes less active as the cancer progresses (comprised of 99% and 96% red edges, respectively). On the other hand, figure 6c and 6d can be considered to be functional subnetwork modules which becomes more active as the cancer progresses (both comprised of 99% green edges). Then the network community oncomarker of figure 6e contains a mixture of these effects (comprised of 87% red and 13% green edges). However, each of these network community oncomarkers represents a functional subnetwork module which is rewired in a way which is advantageous for the cancer, in favour of proliferation, and against cell death and immune function. The genes/nodes of these network community oncomarkers are shown in tables S1 - S5; they list many genes related to cell proliferation (e.g., CDKL1, NKAPL, MAPK6), developmental processes (e.g., HOXD10, HOXB9, HOXC10, HOXA13, HOXC12, HOXD13), and immune function (e.g., VSIG2, IL36B, RBPJ).

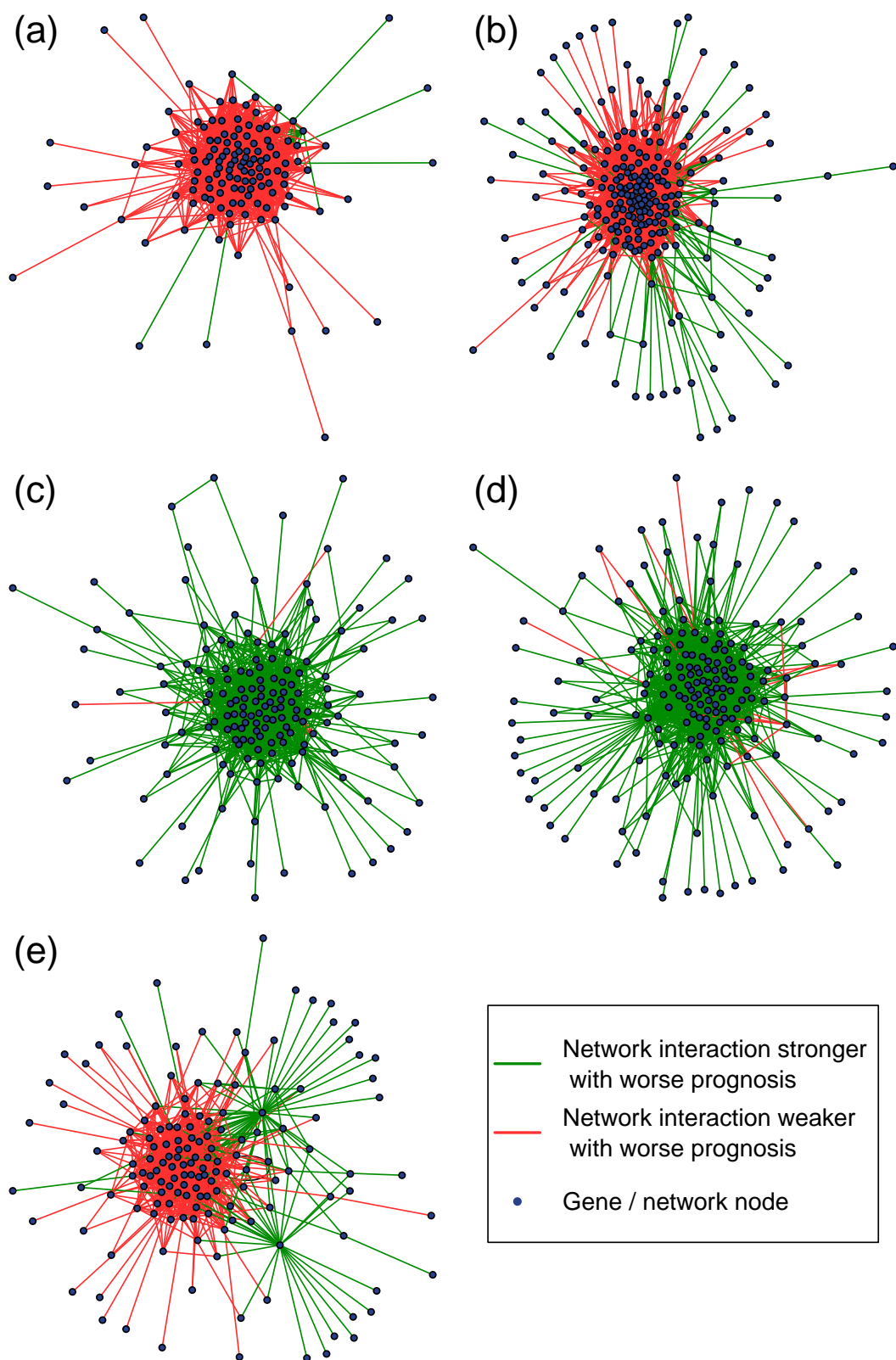


Figure 6: Detected network community oncomarkers.
 (a) - (e) indicate network community oncomarkers 1 - 5, as shown in figure 3.

We hypothesise that the DNA methylation network interaction measure is a reflection of co-regulatory or co-regulated gene-expression patterns, among other genomic effects. We tested this hypothesis by comparing the DNA methylation network interaction measure ρ_{XY} for a pair of genes XY (equation 2) with an equivalent measure of interactive behaviour of these genes in terms of their expression levels, ρ_{XY}^{expr} (equation 12). Correlation test p -values for the comparison between ρ_{XY} and ρ_{XY}^{expr} appear in figure 7. It is clear that in these histograms, there is a concentration of significant p -values close to zero, indicating a departure from the null hypothesis uniform distribution, and demonstrating an association between ρ_{XY} and ρ_{XY}^{expr} for many of the edges/interactions of each network community oncomarker. However, there are also many non-significant p -values visible in these histograms, indicating that there are other genomic interactive effects present which cannot be explained in terms of gene expression (as assessed by mRNA levels) alone. Such effects are expected to include the influence of alternatively spliced products or isoforms [Jones, 2012] and the interaction between non-coding transcripts and the epigenome [Lai and Shiekhhattar, 2014].

4 Discussion

In this paper, we have proposed methodology to detect cancer biomarkers based on the epigenomic pattern DNA methylation. This methodology builds on a measure of pairwise interaction between genes, based on the epigenomic gene-regulatory pattern DNA methylation. Based on this measure, the methodology we have introduced in this paper allows inference of prognostic genomic networks, and identification of prognostic biomarkers from such networks using community detection methodology. We call these ‘network community oncomarkers’; they are groups of nodes/genes among which there is a high density of prognostic genomic interactive or associative behaviour. We have demonstrated that within these communities, the DNA methylation network interaction measure is highly associated with co-regulatory behaviour linked to gene expression (at the mRNA level), giving functional relevance to the findings. However, there are also likely to be a range of genomic interactive effects present which are measured by the DNA methylation network interaction measure but which are not reflected in mRNA levels. Our proposed methodology also allows a one-number prognostic score for a network community oncomarker to be calculated for each patient/sample: this prognostic score is a measure of disease progression in that patient.

Our proposed methodology uses mixture modelling to infer network structure from prognostic association between genes, and draws on practical approaches to community detection to obtain oncomarkers from this prognostic network. Mixture modelling has previously been shown to be an effective approach to the related problem of clustering in networks [Vu et al., 2013]. This suggests that more general methodology could be developed here, in which network and community inference are both carried out simultaneously by model fitting. Network inference has also been carried out previously using multiple node attributes in cell biological data [Katenka et al., 2012], and those findings could be used as a basis upon which data from other genomic sources could be integrated into the methodology proposed here. Genes also frequently carry out multiple roles in different biological contexts and hence may be involved in more than one functional subnetwork module within a genomic network. Work has been carried out on overlapping stochastic blockmodels [Latouche et al., 2011], and hence this would be a natural context in which to develop an application for such methodology.

The field of epigenomics is progressing fast and promises many new insights in the near future into unexplained or undiscovered genomic phenomena, for example relating to the so-called ‘dark matter’ of the genome [Venters and Pugh, 2013]. Epigenomics is also expected to provide new understanding of the mechanisms of disease progression. The discovery that some genomic loci gain or lose methylation in ways which may be unique to cancer suggests that understanding changes in DNA methylation machinery may be essential to understanding oncogenesis [Xie et al., 2013]. The field of network science is also advancing rapidly. Networks are an efficient way to represent and analyse large numbers of variables, which is particularly relevant in modern, large-scale genomic studies. Networks of interactions are a natural way to represent and analyse genomic interactions, associations and processes. Therefore, the study of genomic and epigenomic networks promises to be productive over the coming years for the fields of biology, medicine, statistics.

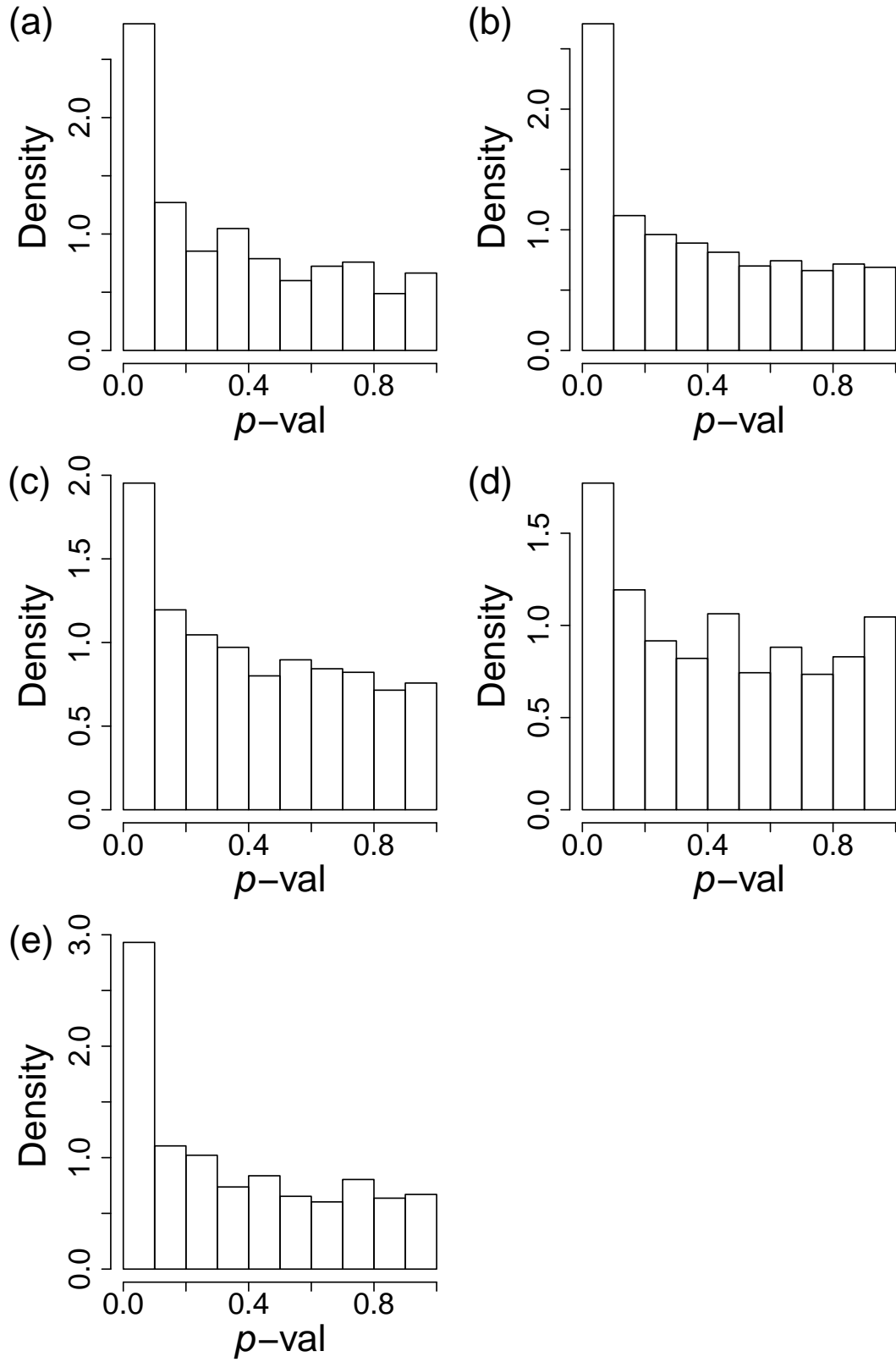


Figure 7: Correlation of DNA methylation with gene expression for the network community oncomarkers. (a) - (e) indicate network community oncomarkers 1 - 5, as shown in figure 3.

References

- A.-L. Barabási and Z. N. Oltvai. Network biology: understanding the cell’s functional organization. *Nature Reviews Genetics*, 5(2):101–113, 2004.
- T. E. Bartlett. Network inference and community detection, based on covariance matrices, correlations and test statistics from arbitrary distributions. *arXiv preprint arXiv:1506.04928*, 2015.
- T. E. Bartlett, A. Zaikin, S. C. Olhede, J. West, A. E. Teschendorff, and M. Widschwendter. Corruption of the intra-gene DNA methylation architecture is a hallmark of cancer. *PloS One*, 8(7):e68285, 2013.
- T. E. Bartlett, S. C. Olhede, and A. Zaikin. A DNA methylation network interaction measure, and detection of network oncomarkers. *PloS One*, 9(1):e84573, 2014.
- M. Beguerisse-Díaz, G. Garduño-Hernández, B. Vangelov, S. N. Yaliraki, and M. Barahona. Interest communities and flow roles in directed networks: the twitter network of the uk riots. *Journal of The Royal Society Interface*, 11(101):20140940, 2014.
- R. Bhagat, S. Chadaga, C. Premalata, G. Ramesh, C. Ramesh, V. Pallavi, and L. Krishnamoorthy. Aberrant promoter methylation of the rassfla and apc genes in epithelial ovarian carcinoma development. *Cellular Oncology*, 35(6):473–479, 2012.
- P. J. Bickel and A. Chen. A nonparametric view of network models and newman–girvan and other modularities. *Proceedings of the National Academy of Sciences*, 106(50):21068–21073, 2009.
- L. Bonetta. Genome sequencing in the fast lane. *Nature Methods*, 3(2):141, 2006.
- D. Brocks, Y. Assenov, S. Minner, O. Bogatyrova, R. Simon, C. Koop, C. Oakes, M. Zucknick, D. B. Lipka, J. Weischenfeldt, et al. Intratumor DNA methylation heterogeneity reflects clonal evolution in aggressive prostate cancer. *Cell reports*, 8(3):798–806, 2014.
- B. C. Christensen, E. A. Houseman, C. J. Marsit, S. Zheng, M. R. Wrensch, J. L. Wiemels, H. H. Nelson, M. R. Karagas, J. F. Padbury, R. Bueno, et al. Aging and environmental exposures alter tissue-specific DNA methylation dependent upon CpG island context. *PLoS Genetics*, 5(8):e1000602, 2009.
- F. Collins and A. Barker. Mapping the cancer genome. *Scientific American Magazine*, 296(3):50–57, 2007.
- C. A. Cooney. Epigenetics-DNA-based mirror of our environment? *Disease Markers*, 23(1):121–137, 2007.
- D. R. Cox. Regression models and life tables (with discussion). *Journal of the Royal Statistical Society*, 34:187–220, 1972.
- A. Feinberg, R. Ohlsson, and S. Henikoff. The epigenetic progenitor origin of human cancer. *Nature Reviews Genetics*, 7(1):21–33, 2006.
- T. Fleischer, A. Frigessi, K. C. Johnson, H. Edvardsen, N. Touleimat, J. Klajic, M. L. Riis, V. Haakensen, F. Wärnberg, B. Naume, et al. Genome-wide DNA methylation profiles in progression to in situ and invasive carcinoma of the breast with impact on gene transcription and prognosis. *Genome Biol*, 15: 435, 2014.
- F. Gao, L. Shi, J. Russin, L. Zeng, X. Chang, S. He, T. C. Chen, S. L. Giannotta, D. J. Weisenberger, G. Zada, et al. DNA methylation in the malignant transformation of meningiomas. *PloS One*, 8(1): e54114, 2013.
- M. Girvan and M. E. Newman. Community structure in social and biological networks. *Proceedings of the National Academy of Sciences*, 99(12):7821–7826, 2002.
- T. Hampton. Cancer genome atlas. *JAMA: The Journal of the American Medical Association*, 296(16): 1958–1958, 2006.

- F. E. Harrell. *Regression modeling strategies: with applications to linear models, logistic regression, and survival analysis*. Springer, 2001.
- P. W. Holland, K. B. Laskey, and S. Leinhardt. Stochastic blockmodels: First steps. *Social networks*, 5(2):109–137, 1983.
- H. Hotelling. Relations between two sets of variates. *Biometrika*, 28(3/4):321–377, 1936.
- L. Jacob, P. Neuvial, S. Dudoit, et al. More power via graph-structured tests for differential expression of gene networks. *The Annals of Applied Statistics*, 6(2):561–600, 2012.
- I. M. Johnstone and B. W. Silverman. Needles and straw in haystacks: Empirical bayes estimates of possibly sparse sequences. *Annals of Statistics*, pages 1594–1649, 2004.
- P. Jones. Functions of DNA methylation: islands, start sites, gene bodies and beyond. *Nature Reviews Genetics*, 13(7):484–492, 2012.
- G. H. Kang, Y.-H. Shim, H.-Y. Jung, W. H. Kim, J. Y. Ro, and M.-G. Rhyu. CpG island methylation in premalignant stages of gastric carcinoma. *Cancer research*, 61(7):2847–2851, 2001.
- G. H. Kang, S. Lee, J.-S. Kim, and H.-Y. Jung. Profile of aberrant CpG island methylation along multistep gastric carcinogenesis. *Laboratory investigation*, 83(4):519–526, 2003.
- N. Katenka, E. D. Kolaczyk, et al. Inference and characterization of multi-attribute networks with application to computational biology. *The Annals of Applied Statistics*, 6(3):1068–1094, 2012.
- Y. Kishida, A. Natsume, Y. Kondo, I. Takeuchi, B. An, Y. Okamoto, K. Shinjo, K. Saito, H. Ando, F. Ohka, et al. Epigenetic subclassification of meningiomas based on genome-wide DNA methylation analyses. *Carcinogenesis*, 33(2):436–441, 2012.
- F. Lai and R. Shiekhattar. Where long noncoding rnas meet dna methylation. *Cell research*, 24(3):263–264, 2014.
- P. Latouche, E. Birmelé, C. Ambroise, et al. Overlapping stochastic block models with application to the french political blogosphere. *The Annals of Applied Statistics*, 5(1):309–336, 2011.
- C. Li and J. Wang. Quantifying the underlying landscape and paths of cancer. *Journal of The Royal Society Interface*, 11(100):20140774, 2014.
- Y. Luo, C.-J. Wong, A. M. Kaz, S. Dzieciatkowski, K. T. Carter, S. M. Morris, J. Wang, J. E. Willis, K. W. Makar, C. M. Ulrich, et al. Differences in DNA methylation signatures reveal multiple pathways of progression from adenoma to colorectal cancer. *Gastroenterology*, 2014.
- R. Maekawa, S. Sato, Y. Yamagata, H. Asada, I. Tamura, L. Lee, M. Okada, H. Tamura, E. Takaki, A. Nakai, et al. Genome-wide DNA methylation analysis reveals a potential mechanism for the pathogenesis and development of uterine leiomyomas. *PloS One*, 8(6):e66632, 2013.
- K. V. Mardia. Statistical approaches to three key challenges in protein structural bioinformatics. *Journal of the Royal Statistical Society: Series C (Applied Statistics)*, 62(3):487–514, 2013.
- A. K. Nandi, A. Sumana, and K. Bhattacharya. Social insect colony as a biological regulatory system: modelling information flow in dominance networks. *Journal of The Royal Society Interface*, 11(101):20140951, 2014.
- A. Navarro, P. Yin, D. Monsivais, S. M. Lin, P. Du, J.-J. Wei, and S. E. Bulun. Genome-wide DNA methylation indicates silencing of tumor suppressor genes in uterine leiomyoma. *PloS One*, 7(3):e33284, 2012.
- M. E. Newman. Detecting community structure in networks. *The European Physical Journal B-Condensed Matter and Complex Systems*, 38(2):321–330, 2004.
- M. E. Newman and M. Girvan. Finding and evaluating community structure in networks. *Physical review E*, 69(2):026113, 2004.

- S. C. Olhede and P. J. Wolfe. Network histograms and universality of blockmodel approximation. *Proceedings of the National Academy of Sciences*, 111(41):14722–14727, 2014. doi: 10.1073/pnas.1400374111. URL <http://www.pnas.org/content/111/41/14722.abstract>.
- G. Palla, L. Lovász, and T. Vicsek. Multifractal network generator. *Proceedings of the National Academy of Sciences*, 107(17):7640–7645, 2010.
- T. Qin and K. Rohe. Regularized spectral clustering under the degree-corrected stochastic blockmodel. In *Advances in Neural Information Processing Systems*, pages 3120–3128, 2013.
- E. Reznik, A. Watson, and O. Chaudhary. The stubborn roots of metabolic cycles. *Journal of The Royal Society Interface*, 10(83):20130087, 2013.
- M. A. Riolo and M. Newman. First-principles multiway spectral partitioning of graphs. *arXiv preprint arXiv:1209.5969*, 2012.
- S. Saavedra, R. P. Rohr, L. J. Gilarranz, and J. Bascompte. How structurally stable are global socio-economic systems? *Journal of The Royal Society Interface*, 11(100):20140693, 2014.
- S. S. Shen-Orr, R. Milo, S. Mangan, and U. Alon. Network motifs in the transcriptional regulation network of escherichia coli. *Nature Genetics*, 31(1):64–68, 2002.
- I. W. Taylor, R. Linding, D. Warde-Farley, Y. Liu, C. Pesquita, D. Faria, S. Bull, T. Pawson, Q. Morris, and J. L. Wrana. Dynamic modularity in protein interaction networks predicts breast cancer outcome. *Nature biotechnology*, 27(2):199–204, 2009.
- T.-D. Tran and Y.-K. Kwon. The relationship between modularity and robustness in signalling networks. *Journal of The Royal Society Interface*, 10(88):20130771, 2013.
- A. Van Hoesel, Y. Sato, D. Elashoff, R. Turner, A. Giuliano, J. Shamonki, P. Kuppen, C. van de Velde, and D. Hoon. Assessment of DNA methylation status in early stages of breast cancer development. *British journal of cancer*, 108(10):2033–2038, 2013.
- B. J. Venters and B. F. Pugh. Genomic organization of human transcription initiation complexes. *Nature*, 502(7469):53–58, 2013.
- A. H. Verschuur-Maes, P. C. de Bruin, and P. J. van Diest. Epigenetic progression of columnar cell lesions of the breast to invasive breast cancer. *Breast cancer research and treatment*, 136(3):705–715, 2012.
- D. Q. Vu, D. R. Hunter, M. Schweinberger, et al. Model-based clustering of large networks. *The Annals of Applied Statistics*, 7(2):1010–1039, 2013.
- A. Wagner. Estimating coarse gene network structure from large-scale gene perturbation data. *Genome Research*, 12(2):309–315, 2002.
- P. Wei and W. Pan. Network-based genomic discovery: application and comparison of markov random-field models. *Journal of the Royal Statistical Society: Series C (Applied Statistics)*, 59(1):105–125, 2010.
- W. Xie, M. D. Schultz, R. Lister, Z. Hou, N. Rajagopal, P. Ray, J. W. Whitaker, S. Tian, R. D. Hawkins, D. Leung, et al. Epigenomic analysis of multilineage differentiation of human embryonic stem cells. *Cell*, 153(5):1134–1148, 2013.
- E. Yamamoto, H. Suzuki, H.-o. Yamano, R. Maruyama, M. Nojima, S. Kamimae, T. Sawada, M. Ashida, K. Yoshikawa, T. Kimura, et al. Molecular dissection of premalignant colorectal lesions reveals early onset of the CpG island methylator phenotype. *The American journal of pathology*, 181(5):1847–1861, 2012.

Data-sets

DNA methylation (DNAm) data from breast cancer invasive carcinoma (BRCA) tumour samples, collected via the Illumina Infinium HumanMethylation450 platform, were downloaded from The Cancer Genome Atlas (TCGA) project [Hampton, 2006, Bonetta, 2006, Collins and Barker, 2007] at level 3. These data were pre-processed by first removing probes with non-unique mappings and which map to SNPs (as identified in the TCGA level 3 data); probes mapping to sex chromosomes were also removed; in total 98384 probes were removed in this way from all data sets. After removal of these probes, 270985 probes with known gene annotations remained. Probes were then removed if they had less than 95% coverage across samples; probe values were also replaced if they had corresponding detection p -value greater than 5%, by KNN (k nearest neighbour) imputation ($k = 5$). The loci of analysed CpGs were mapped to genes based on annotation information for the Illumina Infinium platform obtained from the *R* / *Bioconductor* package ‘IlluminaHumanMethylation450k’. The data were also checked for batch effects by hierarchical clustering and correlation of the significant principle components with phenotype and batch: no significant batch effects (which would warrant further correction) were found. We downloaded DNA methylation data for tumour samples from 175 samples/individuals, from TCGA in July 2013, with clinical data available for patient survival outcome, and the clinical covariates age, disease stage, and residual disease. At the same time, we also downloaded corresponding DNA methylation data for healthy tissue for 98 individuals. These data were used to detect potential network community oncomarkers. We then downloaded DNA methylation data for a further 528 tumour samples from TCGA in September 2014, with data for the same clinical features available. These independent samples were used to validate the potential network community oncomarkers. At this time we also downloaded gene expression data from TCGA at level 3, for 216 of the tumours for which we also obtained DNA methylation data.

Acknowledgements

TB acknowledges support from the UK EPSRC and MRC via UCL CoMPLEX. AZ acknowledges support from the Deanship of Scientific Research (DSR), King Abdulaziz University (KAU), Jeddah, under grant No. (86-130-35-RG) and from the Russian Foundation for Basic Research (14-02-01202,13-02-00918).

Supplementary tables

Degree	Gene/node	Chr	Gene info
93	POR	7	P450 (cytochrome) oxidoreductase
87	TTF1	9	transcription termination factor, RNA polymerase I
79	ZFFM2	8	zinc finger protein, FOG family member 2
79	ARHGAP21	10	Rho GTPase activating protein 21
77	VSIG2	11	V-set and immunoglobulin domain containing 2
74	P4HA1	10	prolyl 4-hydroxylase, alpha polypeptide 1
73	MSLNL	16	mesothelin-like
71	COASY	17	CoA synthase
71	FBLL1	5	fibrillarlin-like 1
68	ANXA2	15	annexin A2
65	CERS4	19	ceramide synthase 4
63	ZNF469	16	zinc finger protein 469
63	SYNGR3	16	synaptogyrin 3
63	FXYP1	19	FXYP domain containing ion transport regulator 1
63	IZUMO1	19	izumo sperm-egg fusion 1
61	EXOC2	6	exocyst complex component 2
60	RAP1GAP	1	RAP1 GTPase activating protein
60	PAK1	11	p21 protein (Cdc42/Rac)-activated kinase 1
59	DRD4	11	dopamine receptor D4
59	TAF5L	1	TAF5-like RNA polymerase II, p300/CBP-associated factor (PCAF)-associated factor, 65kDa
58	SHOX2	3	short stature homeobox 2
58	HOXB9	17	homeobox B9
57	TACR1	2	tachykinin receptor 1
57	DCHS1	11	dachsous cadherin-related 1
56	RTP3	3	receptor (chemosensory) transporter protein 3
55	DDX52	17	DEAD (Asp-Glu-Ala-Asp) box polypeptide 52
54	SNX32	11	sorting nexin 32
54	TLE1	9	transducin-like enhancer of split 1 (E(sp1) homolog, Drosophila)
53	CNNM4	2	cyclin M4
53	CNIH2	11	cornichon family AMPA receptor auxiliary protein 2
53	LOC400940	2	uncharacterized LOC400940
53	MAPK3	16	mitogen-activated protein kinase 3
52	RB1	13	retinoblastoma 1
52	FUCA1	1	fucosidase, alpha-L- 1, tissue
50	PPP2R5C	14	protein phosphatase 2, regulatory subunit B', gamma
50	B3GALT1	13	beta 1,3-galactosyltransferase-like
48	JAK3	19	Janus kinase 3
47	SLC25A42	19	solute carrier family 25, member 42
46	TTC22	1	tetratricopeptide repeat domain 22
46	NPDC1	9	neural proliferation, differentiation and control, 1
45	ASB4	7	ankyrin repeat and SOCS box containing 4
45	ALDH2	12	aldehyde dehydrogenase 2 family (mitochondrial)
45	ZNF296	19	zinc finger protein 296
44	RBPJ	4	recombination signal binding protein for immunoglobulin kappa J region
44	NAT8L	4	N-acetyltransferase 8-like (GCN5-related, putative)
44	SMPDL3A	6	sphingomyelin phosphodiesterase, acid-like 3A
42	KLHL26	19	kelch-like family member 26
41	EBF4	20	early B-cell factor 4
41	SLAIN1	13	SLAIN motif family, member 1
41	GAMT	19	guanidinoacetate N-methyltransferase
41	SH2D3A	19	SH2 domain containing 3A
40	BLVRA	7	biliverdin reductase A
39	CD36	7	CD36 molecule (thrombospondin receptor)
39	BAZ1A	14	bromodomain adjacent to zinc finger domain, 1A
39	MLL5	7	lysine (K)-specific methyltransferase 2E
37	PIK3AP1	10	phosphoinositide-3-kinase adaptor protein 1
36	ITGB1BP1	2	integrin beta 1 binding protein 1
34	CMKLR1	12	chemokine-like receptor 1
33	TRIM71	3	tripartite motif containing 71, E3 ubiquitin protein ligase
31	SMAD3	15	SMAD family member 3
31	KIF13B	8	kinesin family member 13B
30	ARID3A	19	AT rich interactive domain 3A (BRIGHT-like)
30	F2R	5	coagulation factor II (thrombin) receptor
30	AMN1	12	antagonist of mitotic exit network 1 homolog (S. cerevisiae)
29	LOC100128239	11	uncharacterized LOC100128239
29	LRRC8B	1	leucine rich repeat containing 8 family, member B
29	ANKRD39	2	ankyrin repeat domain 39
29	ARFGAP3	22	ADP-ribosylation factor GTPase activating protein 3
29	RBM28	7	RNA binding motif protein 28
28	ABR	17	active BCR-related
28	CALU	7	calumenin
28	BRPF1	3	bromodomain and PHD finger containing, 1
28	C17orf104	17	chromosome 17 open reading frame 104
28	PAQR3	4	progesterone and adipoQ receptor family member III
27	RGL2	6	ral guanine nucleotide dissociation stimulator-like 2
27	WAC	10	WW domain containing adaptor with coiled-coil
27	PMVK	1	phosphomevalonate kinase
27	PPP6R3	11	protein phosphatase 6, regulatory subunit 3
26	PPP2R1B	11	protein phosphatase 2, regulatory subunit A, beta
25	TOLLIP	11	toll interacting protein
25	RNASEH2A	19	ribonuclease H2, subunit A
24	RERE	1	arginine-glutamic acid dipeptide (RE) repeats
23	KRT27	17	keratin 27
21	B4GALNT2	17	beta-1,4-N-acetyl-galactosaminyl transferase 2
21	MYCBPAP	17	MYCBP associated protein
20	ADCK2	7	aarF domain containing kinase 2
20	ZNF138	7	zinc finger protein 138
19	CDYL	6	chromodomain protein, Y-like
19	SMPD3	16	sphingomyelin phosphodiesterase 3, neutral membrane (neutral sphingomyelinase II)
19	F7	13	coagulation factor VII (serum prothrombin conversion accelerator)
19	SYTL1	1	synaptotagmin-like 1
18	HSPA12B	20	heat shock 70kD protein 12B
18	RAP1GDS1	4	RAP1, GTP-GDP dissociation stimulator 1
18	FABP4	8	fatty acid binding protein 4, adipocyte
17	ARG2	14	arginase 2
17	TSHZ1	18	teashirt zinc finger homeobox 1
17	CAPRN2	12	caprin family member 2
17	CASD1	7	CAS1 domain containing 1
16	MYL9	20	myosin, light chain 9, regulatory
15	CCDC108	2	coiled-coil domain containing 108

Table S1: Network Community Oncomarker 1 (figure 3a) - gene/node info.
The 100 highest degree nodes only are shown.

Degree	Gene/node	Chr	Gene info
137	TMEM198	2	transmembrane protein 198
121	POMP	13	proteasome maturation protein
108	GLT25D1		
107	HMOX1	22	heme oxygenase (decycling) 1
100	STK4	20	serine/threonine kinase 4
94	C1orf38		
90	XPO4	13	exportin 4
83	SOX5	12	SRY (sex determining region Y)-box 5
82	ADRA1B	5	adrenoceptor alpha 1B
81	RIMKLB	12	ribosomal modification protein rimK-like family member B
80	SMG6	17	SMG6 nonsense mediated mRNA decay factor
72	PHLDB1	11	pleckstrin homology-like domain, family B, member 1
72	PLTP	20	phospholipid transfer protein
72	C10orf32	10	chromosome 10 open reading frame 32
71	DLG4	17	discs, large homolog 4 (Drosophila)
67	SLC27A3	1	solute carrier family 27 (fatty acid transporter), member 3
66	KIAA1462	10	KIAA1462
66	FES	15	feline sarcoma oncogene
66	NDEL1	17	nudE neurodevelopment protein 1-like 1
65	ERGIC1	5	endoplasmic reticulum-golgi intermediate compartment (ERGIC) 1
63	FTSJD2	6	cap methyltransferase 1
62	EEPDI	7	endonuclease/exonuclease/phosphatase family domain containing 1
61	KCNA3	1	potassium voltage-gated channel, shaker-related subfamily, member 3
60	BREA2	8	breast cancer estrogen-induced apoptosis 2
59	MAGI2	7	membrane associated guanylate kinase, WW and PDZ domain containing 2
59	NPFF	12	neuropeptide FF-amide peptide precursor
57	SPRYD3	12	SPRY domain containing 3
57	WDR48	3	WD repeat domain 48
56	UHRF1BP1L	12	UHRF1 binding protein 1-like
55	ID1	20	inhibitor of DNA binding 1, dominant negative helix-loop-helix protein
55	GABRA4	4	gamma-aminobutyric acid (GABA) A receptor, alpha 4
55	RNASE1	14	ribonuclease, RNase A family, 1 (pancreatic)
54	CDKL1	14	cyclin-dependent kinase-like 1 (CDC2-related kinase)
54	MAP4K1	19	mitogen-activated protein kinase kinase kinase kinase 1
54	TRADD	16	TNFRSF1A-associated via death domain
52	LOXL2	8	lysyl oxidase-like 2
52	CARS	11	cysteinyI-tRNA synthetase
51	NR3C1	5	nuclear receptor subfamily 3, group C, member 1 (glucocorticoid receptor)
51	SPEF2	5	sperm flagellar 2
51	LSM14B	20	LSM14B, SCD6 homolog B (S. cerevisiae)
50	LRBA	4	LPS-responsive vesicle trafficking, beach and anchor containing
50	LOC440910	2	uncharacterized LOC440910
49	SELO	22	selenoprotein O
46	TAOK1	17	TAO kinase 1
46	DNPEP	2	aspartyl aminopeptidase
43	HOXD10	2	homeobox D10
43	HGSNAT	8	heparan-alpha-glucosaminide N-acetyltransferase
43	ERMAP	1	erythroblast membrane-associated protein (Scianna blood group)
43	PPAP2A	5	phosphatidic acid phosphatase type 2A
40	MAML3	4	mastermind-like 3 (Drosophila)
40	FBXO4	5	F-box protein 4
40	SFT2D1	6	SFT2 domain containing 1
39	RIN2	20	Ras and Rab interactor 2
38	SYCP1	1	synaptonemal complex protein 1
37	PLBD1	12	phospholipase B domain containing 1
36	PRKCG	19	protein kinase C, gamma
36	ANKMY1	2	ankyrin repeat and MYND domain containing 1
36	ADAM19	5	ADAM metalloproteinase domain 19
35	PARD3	10	par-3 family cell polarity regulator
35	EXOC3	5	exocyst complex component 3
33	TTYH3	7	tweety family member 3
33	PIGG	4	phosphatidylinositol glycan anchor biosynthesis, class G
33	PFDN1	5	prefoldin subunit 1
32	PCDH8	13	protocadherin 8
32	PCBD2	5	pterin-4 alpha-carbinolamine dehydratase/dimerization cofactor of hepatocyte nuclear factor 1 alpha (TCF1) 2
32	NR1H3	11	nuclear receptor subfamily 1, group H, member 3
32	CTAGE1	18	cutaneous T-cell lymphoma-associated antigen 1
31	SOX14	3	SRY (sex determining region Y)-box 14
31	LRRC41	1	leucine rich repeat containing 41
30	PTPLAD1	15	protein tyrosine phosphatase-like A domain containing 1
30	ARMC2	6	armadillo repeat containing 2
30	BMP2	20	bone morphogenetic protein 2
29	NKAPL	6	NFKB activating protein-like
28	CCDC17	1	coiled-coil domain containing 17
27	ARL5C	17	ADP-ribosylation factor-like 5C
27	CECR6	22	cat eye syndrome chromosome region, candidate 6
27	SH3BGR1L3	1	SH3 domain binding glutamate-rich protein like 3
26	TMEM51	1	transmembrane protein 51
26	C1QL3	10	complement component 1, q subcomponent-like 3
26	GPANK1	6	G patch domain and ankyrin repeats 1
25	KIAA0226	3	KIAA0226
23	GGT7	20	gamma-glutamyltransferase 7
23	ZNF837	19	zinc finger protein 837
22	VPS13D	1	vacuolar protein sorting 13 homolog D (S. cerevisiae)
22	SLC12A4	16	solute carrier family 12 (potassium/chloride transporter), member 4
22	GTF3C1	16	general transcription factor IIC, polypeptide 1, alpha 220kDa
22	C17orf82	17	chromosome 17 open reading frame 82
22	FUT9	6	fucosyltransferase 9 (alpha (1,3) fucosyltransferase)
22	C5orf4	5	fatty acid hydroxylase domain containing 2
21	MCF2L	13	MCF 2 cell line derived transforming sequence-like
21	GSN	9	gelsolin
21	NIPAL2	8	NIPA-like domain containing 2
21	MIR663A	20	microRNA 663a
21	CALB1	8	calbindin 1, 28kDa
20	ZSCAN12	6	zinc finger and SCAN domain containing 12
20	KCNA2	1	potassium voltage-gated channel, shaker-related subfamily, member 2
20	EXD2	14	exonuclease 3'-5' domain containing 2
20	PDZD7	10	PDZ domain containing 7
20	HIST1H3J	6	histone cluster 1, H3j
18	PLEKHB1	11	pleckstrin homology domain containing, family B (evectins) member 1

Table S2: Network Community Oncomarker 2 (figure 3b) - gene/node info.
The 100 highest degree nodes only are shown.

Degree	Gene/node	Chr	Gene info
60	SOD2	6	superoxide dismutase 2, mitochondrial
56	ULK1	12	unc-51 like autophagy activating kinase 1
56	IL36B	2	interleukin 36, beta
47	GOLGA8A	15	golgin A8 family, member A
44	C14orf162		
44	DDX27	20	DEAD (Asp-Glu-Ala-Asp) box polypeptide 27
44	MRPL35	2	mitochondrial ribosomal protein L35
43	ZNF202	11	zinc finger protein 202
43	JUND	19	jun D proto-oncogene
43	PAPD4	5	PAP associated domain containing 4
42	ASF1B	19	anti-silencing function 1B histone chaperone
41	SLC35E3	12	solute carrier family 35, member E3
41	USF1	1	upstream transcription factor 1
41	AXDND1	1	axonemal dynein light chain domain containing 1
40	PAFAH1B2	11	platelet-activating factor acetylhydrolase 1b, catalytic subunit 2 (30kDa)
39	ZNF2	2	zinc finger protein 2
39	KIF2C	1	kinesin family member 2C
37	SOX4	6	SRY (sex determining region Y)-box 4
37	CNIH4	1	cornichon family AMPA receptor auxiliary protein 4
37	TDRD12	19	tudor domain containing 12
36	IFNGR2	21	interferon gamma receptor 2 (interferon gamma transducer 1)
35	NMI	2	N-myc (and STAT) interactor
35	ADAM29	4	ADAM metalloproteinase domain 29
34	DNAJC16	1	DnaJ (Hsp40) homolog, subfamily C, member 16
32	GSR	8	glutathione reductase
32	RPL5	1	ribosomal protein L5
32	C16orf79		
31	C13orf35	13	ATP11A upstream neighbor
30	SLC7A5	16	solute carrier family 7 (amino acid transporter light chain, L system), member 5
30	ATXN2	12	ataxin 2
30	KLC4	6	kinesin light chain 4
29	TMEM8A	16	transmembrane protein 8A
29	DCLRE1C	10	DNA cross-link repair 1C
28	ORAI1	12	ORAI calcium release-activated calcium modulator 1
28	MTHFS	15	5,10-methylenetetrahydrofolate synthetase (5-formyltetrahydrofolate cyclo-ligase)
27	GRIA4	11	glutamate receptor, ionotropic, AMPA 4
27	DDA1	19	DET1 and DDB1 associated 1
27	SDF2L1	22	stromal cell-derived factor 2-like 1
27	HIST1H2AB	6	histone cluster 1, H2ab
26	P2RX1	17	purinergic receptor P2X, ligand-gated ion channel, 1
26	SLC22A1	6	solute carrier family 22 (organic cation transporter), member 1
26	FBXL12	19	F-box and leucine-rich repeat protein 12
25	SCLY	2	selenocysteine lyase
25	HFM1	1	HFM1, ATP-dependent DNA helicase homolog (S. cerevisiae)
24	CHRM3	1	cholinergic receptor, muscarinic 3
23	ZNF764	16	zinc finger protein 764
23	LEO1	15	Leo1, Paf1/RNA polymerase II complex component, homolog (S. cerevisiae)
23	MARC1	1	mitochondrial amidoxime reducing component 1
22	CAPRIN1	11	cell cycle associated protein 1
22	RAB11A	15	RAB11A, member RAS oncogene family
22	CCNI	4	cyclin I
22	PARP14	3	poly (ADP-ribose) polymerase family, member 14
22	RIPK3	14	receptor-interacting serine-threonine kinase 3
22	VCP	9	valosin containing protein
21	SKAP2	7	src kinase associated phosphoprotein 2
21	AGTR1	3	angiotensin II receptor, type 1
21	TMEM45B	11	transmembrane protein 45B
21	NEFL	8	neurofilament, light polypeptide
21	TWF2	3	twinfilin actin-binding protein 2
21	C6orf141	6	chromosome 6 open reading frame 141
21	LOC442308		
21	TRIM21	11	tripartite motif containing 21
20	ADSL	22	adenylosuccinate lyase
19	WDR54	2	WD repeat domain 54
19	GMPPB	3	GDP-mannose pyrophosphorylase B
19	RECK	9	reversion-inducing-cysteine-rich protein with kazal motifs
19	NDUFS5	1	NADH dehydrogenase (ubiquinone) Fe-S protein 5, 15kDa (NADH-coenzyme Q reductase)
18	SLC39A7	6	solute carrier family 39 (zinc transporter), member 7
17	CPT1C	19	carnitine palmitoyltransferase 1C
16	PAFAH2	1	platelet-activating factor acetylhydrolase 2, 40kDa
16	NOS2	17	nitric oxide synthase 2, inducible
15	ING3	7	inhibitor of growth family, member 3
14	HOXC10	12	homeobox C10
13	UPF1	19	UPF1 regulator of nonsense transcripts homolog (yeast)
13	PKHD1	6	polycystic kidney and hepatic disease 1 (autosomal recessive)
13	NCKAP5L	12	NCK-associated protein 5-like
12	CEBPE	14	CCAAT/enhancer binding protein (C/EBP), epsilon
12	USP20	9	ubiquitin specific peptidase 20
12	ST6GALNAC1	17	ST6 (alpha-N-acetyl-neuraminyl-2,3-beta-galactosyl-1,3)-N-acetylgalactosaminide alpha-2,6-sialyltransferase 1
11	ABHD16B	20	abhydrolase domain containing 16B
11	REXO1L2P	8	REX1, RNA exonuclease 1 homolog (S. cerevisiae)-like 2 (pseudogene)
10	NHP2L1	22	NHP2 non-histone chromosome protein 2-like 1 (S. cerevisiae)
10	GANAB	11	glucosidase, alpha; neutral AB
10	PKD1L2	16	polycystic kidney disease 1-like 2
10	CDR2	16	cerebellar degeneration-related protein 2, 62kDa
10	CEACAM8	19	carcinoembryonic antigen-related cell adhesion molecule 8
9	NUP93	16	nucleoporin 93kDa
9	PNMA2	8	paraneoplastic Ma antigen 2
9	C3orf75		
9	ZNF432	19	zinc finger protein 432
9	SEC16B	1	SEC16 homolog B (S. cerevisiae)
9	XRN1	3	5'-3' exoribonuclease 1
9	HIST1H4K	6	histone cluster 1, H4k
8	FOXL1	16	forkhead box L1
8	NOTCH2	1	notch 2
7	ITFG2	12	integrin alpha FG-GAP repeat containing 2
7	METTL21A	2	methyltransferase like 21A
7	FFAR1	19	free fatty acid receptor 1
7	RNF122	8	ring finger protein 122
6	NASP	1	nuclear autoantigenic sperm protein (histone-binding)

Table S3: Network Community Oncomarker 3 (figure 3c) - gene/node info.
The 100 highest degree nodes only are shown.

Degree	Gene/node	Chr	Gene info
74	NOI3	16	nucleolar protein 3 (apoptosis repressor with CARD domain)
72	NAPRT1	8	nicotinate phosphoribosyltransferase domain containing 1
72	PAH	12	phenylalanine hydroxylase
69	POU2F3	11	POU class 2 homeobox 3
67	SNCA	4	synuclein, alpha (non A4 component of amyloid precursor)
66	HOXA13	7	homeobox A13
63	HOXC12	12	homeobox C12
60	WFDC12	20	WAP four-disulfide core domain 12
58	HMG20B	19	high mobility group 20B
51	SAMD3	6	sterile alpha motif domain containing 3
51	SLC10A2	13	solute carrier family 10 (sodium/bile acid cotransporter), member 2
49	ZNF804B	7	zinc finger protein 804B
48	NKX6-1	4	NK6 homeobox 1
48	TEX19	17	testis expressed 19
47	SLC32A1	20	solute carrier family 32 (GABA vesicular transporter), member 1
47	DSC3	18	desmocollin 3
47	CCDC134	22	coiled-coil domain containing 134
47	BDH2	4	3-hydroxybutyrate dehydrogenase, type 2
46	ABCG4	11	ATP-binding cassette, sub-family G (WHITE), member 4
46	VPS41	7	vacuolar protein sorting 41 homolog (S. cerevisiae)
45	SIX1	14	SIX homeobox 1
45	O3FAR1		
45	MIR219-2	9	microRNA 219-2
44	LHX5	12	LIM homeobox 5
44	TARS	5	threonyl-tRNA synthetase
44	C6orf221		
44	C1orf100	1	chromosome 1 open reading frame 100
43	PDX1	13	pancreatic and duodenal homeobox 1
42	VSX2	14	visual system homeobox 2
41	ACTR2	2	ARP2 actin-related protein 2 homolog (yeast)
41	ASZ1	7	ankyrin repeat, SAM and basic leucine zipper domain containing 1
40	E2F8	11	E2F transcription factor 8
40	DPFA2	3	developmental pluripotency associated 2
39	LINC00461	5	long intergenic non-protein coding RNA 461
38	AP4E1	15	adaptor-related protein complex 4, epsilon 1 subunit
38	GPR150	5	G protein-coupled receptor 150
37	LOC440461	17	Rho GTPase activating protein 27 pseudogene
37	C15orf55	15	NUT midline carcinoma, family member 1
37	WTH3DI	2	RAB6C-like
36	GAD1	2	glutamate decarboxylase 1 (brain, 67kDa)
36	TUBA1C	12	tubulin, alpha 1c
36	FAM123A		
36	TULP2	19	tubby like protein 2
36	C19orf53	19	chromosome 19 open reading frame 53
35	LHX9	1	LIM homeobox 9
35	LINC00520	14	long intergenic non-protein coding RNA 520
34	HOXD13	2	homeobox D13
34	KCTD17	22	potassium channel tetramerization domain containing 17
33	HPX	11	hemopexin
32	CD8B	2	CD8b molecule
31	SH2D1B	1	SH2 domain containing 1B
30	GNDF	5	glial cell derived neurotrophic factor
30	RXFP3	5	relaxin/insulin-like family peptide receptor 3
30	CHMP4B	20	charged multivesicular body protein 4B
29	SPRED1	15	sprouty-related, EVH1 domain containing 1
29	MAPK6	15	mitogen-activated protein kinase 6
28	SLC15A1	13	solute carrier family 15 (oligopeptide transporter), member 1
28	HTR1D	1	5-hydroxytryptamine (serotonin) receptor 1D, G protein-coupled
27	VSTM2L	20	V-set and transmembrane domain containing 2 like
27	HIST3H2BB	1	histone cluster 3, H2bb
26	CLGN	4	calmegin
26	MCART2		
25	DNAJC19	3	DnaJ (Hsp40) homolog, subfamily C, member 19
24	ZNF710	15	zinc finger protein 710
24	CDH7	18	cadherin 7, type 2
23	POLR2C	16	polymerase (RNA) II (DNA directed) polypeptide C, 33kDa
22	LIMS2	2	LIM and senescent cell antigen-like domains 2
22	ZSWIM6	5	zinc finger, SWIM-type containing 6
21	FAM174A	5	family with sequence similarity 174, member A
21	MIR130A	11	microRNA 130a
20	ZFAND6	15	zinc finger, AN1-type domain 6
19	ACTA1	1	actin, alpha 1, skeletal muscle
19	TXNDC11	16	thioredoxin domain containing 11
19	ARF3	12	ADP-ribosylation factor 3
19	SNAIL	20	snail family zinc finger 1
19	C11orf20		
18	FAM195A	16	family with sequence similarity 195, member A
18	PPP1R3G	6	protein phosphatase 1, regulatory subunit 3G
17	ADAP2	17	ArfGAP with dual PH domains 2
16	PAQR5	15	progesterone and adipoQ receptor family member V
16	GLTPD1	1	glycolipid transfer protein domain containing 1
16	SLC4A9	5	solute carrier family 4, sodium bicarbonate cotransporter, member 9
14	BMP7	20	bone morphogenetic protein 7
14	NOP58	2	NOP58 ribonucleoprotein
14	MPND	19	MPN domain containing
13	ANXA4	2	annexin A4
13	GHSR	3	growth hormone secretagogue receptor
13	PRLHR	10	prolactin releasing hormone receptor
13	EMILIN3	20	elastin microfibril interfacer 3
12	CCDC102B	18	coiled-coil domain containing 102B
12	NFKB1B	19	nuclear factor of kappa light polypeptide gene enhancer in B-cells inhibitor, beta
11	SH3BP2	4	SH3-domain binding protein 2
11	DCTD	4	dCMP deaminase
11	FGD6	12	FYVE, RhoGEF and PH domain containing 6
11	RASGRP4	19	RAS guanyl releasing protein 4
11	UBA2	19	ubiquitin-like modifier activating enzyme 2
11	SPINK13	5	serine peptidase inhibitor, Kazal type 13 (putative)
10	MMP15	16	matrix metalloproteinase 15 (membrane-inserted)
10	SLITRK1	13	SLIT and NTRK-like family, member 1
10	ARNTL	11	aryl hydrocarbon receptor nuclear translocator-like

Table S4: Network Community Oncomarker 4 (figure 3d) - gene/node info.
The 100 highest degree nodes only are shown.

Degree	Gene/node	Chr	Gene info
62	C3orf18	3	chromosome 3 open reading frame 18
49	FAR1	11	fatty acyl CoA reductase 1
43	DDAH1	1	dimethylarginine dimethylaminohydrolase 1
43	L3MBTL4	18	l(3)mbt-like 4 (Drosophila)
41	NOVA1	14	neuro-oncological ventral antigen 1
40	SPRY1	4	sprouty homolog 1, antagonist of FGF signaling (Drosophila)
39	MAP3K8	10	mitogen-activated protein kinase kinase kinase 8
39	SERTAD4	1	SERTA domain containing 4
38	TPPP3	16	tubulin polymerization-promoting protein family member 3
37	IGFLR1	19	IGF-like family receptor 1
35	KANSL1L	2	KAT8 regulatory NSL complex subunit 1-like
35	LOC100130417	1	uncharacterized LOC100130417
31	CCHCR1	6	coiled-coil alpha-helical rod protein 1
31	LOX	5	lysyl oxidase
31	PLK3	1	polo-like kinase 3
31	RSL1D1	16	ribosomal L1 domain containing 1
30	KIAA0825	5	KIAA0825
30	SEC22A	3	SEC22 vesicle trafficking protein homolog A (S. cerevisiae)
29	VGLL3	3	vestigial-like family member 3
29	MFN2	1	mitofusin 2
29	TRHR	8	thyrotropin-releasing hormone receptor
29	SIGLECP3		
29	TAAR9	6	trace amine associated receptor 9 (gene/pseudogene)
28	LMO4	1	LIM domain only 4
28	POLE2	14	polymerase (DNA directed), epsilon 2, accessory subunit
27	SNX18	5	sorting nexin 18
26	PHACTR2	6	phosphatase and actin regulator 2
26	SCARB2	4	scavenger receptor class B, member 2
26	PGLS	19	6-phosphogluconolactonase
26	MIR365B	17	microRNA 365b
25	C16orf80	16	chromosome 16 open reading frame 80
25	CDK17	12	cyclin-dependent kinase 17
24	GPM6A	4	glycoprotein M6A
24	SLC35D1	1	solute carrier family 35 (UDP-GlcA/UDP-GalNAc transporter), member D1
24	PMM2	16	phosphomannomutase 2
24	C8orf45		
23	SOAT1	1	sterol O-acyltransferase 1
22	KIFC1	6	kinesin family member C1
22	ZNF8	19	zinc finger protein 8
22	TXNDC15	5	thioredoxin domain containing 15
22	FLJ26850	19	FLJ26850 protein
21	STAT5A	17	signal transducer and activator of transcription 5A
21	ST6GALNAC6	9	ST6 (alpha-N-acetyl-neuraminyl-2,3-beta-galactosyl-1,3)-N-acetylgalactosaminide alpha-2,6-sialyltransferase 6
21	KCTD10	12	potassium channel tetramerization domain containing 10
20	ANKS1A	6	ankyrin repeat and sterile alpha motif domain containing 1A
20	XYLT2	17	xylosyltransferase II
20	NUCB1	19	nucleobindin 1
19	LOC440040	11	glutamate receptor, metabotropic 5 pseudogene
18	HBM	16	hemoglobin, mu
18	ENPP2	8	ectonucleotide pyrophosphatase/phosphodiesterase 2
18	SNX21	20	sorting nexin family member 21
18	KLF1	19	Kruppel-like factor 1 (erythroid)
17	HMGB2	4	high mobility group box 2
17	FOXD1	5	forkhead box D1
16	WDR43	2	WD repeat domain 43
15	STK10	5	serine/threonine kinase 10
15	GSX1	13	GS homeobox 1
14	GRM3	7	glutamate receptor, metabotropic 3
14	LOC285548	4	long intergenic non-protein coding RNA 1096
14	HIST1H4G	6	histone cluster 1, H4g
13	RTN3	11	reticulon 3
13	ATG14	14	autophagy related 14
13	TBC1D3C	17	TBC1 domain family, member 3C
12	FNDC3B	3	fibronectin type III domain containing 3B
12	DNAJCG	1	DnaJ (Hsp40) homolog, subfamily C, member 6
11	YWHAG	7	tyrosine 3-monooxygenase/tryptophan 5-monooxygenase activation protein, gamma
11	NUPL1	13	nucleoporin like 1
10	FHL3	1	four and a half LIM domains 3
10	ANKRD34A	1	ankyrin repeat domain 34A
10	GNB3	12	guanine nucleotide binding protein (G protein), beta polypeptide 3
9	GABRA1	5	gamma-aminobutyric acid (GABA) A receptor, alpha 1
9	MLXIP	12	MLX interacting protein
9	ADORA3	1	adenosine A3 receptor
9	TRIM17	1	tripartite motif containing 17
9	MFGES	15	milk fat globule-EGF factor 8 protein
9	FAM86C2P	11	family with sequence similarity 86, member A pseudogene
9	LACTB	15	lactamase, beta
8	CYB5R3	22	cytochrome b5 reductase 3
8	ATOH7	10	atonal homolog 7 (Drosophila)
8	PRKAA1	5	protein kinase, AMP-activated, alpha 1 catalytic subunit
7	ATXN7	3	ataxin 7
7	IGFN1	1	immunoglobulin-like and fibronectin type III domain containing 1
7	HDHD2	18	haloacid dehalogenase-like hydrolase domain containing 2
7	C14orf39	14	chromosome 14 open reading frame 39
6	VAMP3	1	vesicle-associated membrane protein 3
6	ARGLU1	13	arginine and glutamate rich 1
6	ATP6V0A2	12	ATPase, H+ transporting, lysosomal V0 subunit a2
6	NIPAL1	4	NIPA-like domain containing 1
5	PXN	12	paxillin
5	OLIG2	21	oligodendrocyte lineage transcription factor 2
5	RAB32	6	RAB32, member RAS oncogene family
5	NYNRIN	14	NYN domain and retroviral integrase containing
5	GPR182	12	G protein-coupled receptor 182
4	ITPR1PL1	2	inositol 1,4,5-trisphosphate receptor interacting protein-like 1
4	BHLHE23	20	basic helix-loop-helix family, member e23
4	EIF2B3	1	eukaryotic translation initiation factor 2B, subunit 3 gamma, 58kDa
4	HIST1H4F	6	histone cluster 1, H4f
3	CD2AP	6	CD2-associated protein
3	FITM2	20	fat storage-inducing transmembrane protein 2
2	GNL1	6	guanine nucleotide binding protein-like 1

Table S5: Network Community Oncomarker 5 (figure 3e) - gene/node info.
The 100 highest degree nodes only are shown.